Mapping the Circumstellar Environment of T Tauri with Fluorescent H_2 Emission

Frederick M. Walter

Department of Physics and Astronomy, Stony Brook University, Stony Brook NY 11794-3800
fwalter@astro.sunysb.edu

Gregory Herczeg

JILA, University of Colorado, Boulder, CO 80309-0440
gregoryh@casa.colorado.edu

Alexander Brown

Center for Astrophysics and Space Astronomy, University of Colorado, Boulder CO 80309-0389
ab@casa.colorado.edu

David R. Ardila

Department of Physics & Astronomy, Johns Hopkins University, Baltimore MD, 21218
ardila@pha.jhu.edu

Gösta F. Gahm

Stockholm University, AlbaNova, SE - 106 91 Stockholm, Sweden
gahm@astro.su.se

Christopher M. Johns-Krull

Department of Physics & Astronomy, Rice University, Houston TX 77005-1892
cmj@rice.edu

Jack J. Lissauer

Space Science Division, 245-3, NASA/Ames Research Center, Moffett Field, CA 94035
lissauer@ringside.arc.nasa.gov

Michal Simon

Department of Physics and Astronomy, Stony Brook University, Stony Brook NY 11794-3800
msimon@astro.sunysb.edu

Jeff A. Valenti

Space Telescope Science Institute, Baltimore MD 21218
valenti@stsci.edu

ABSTRACT

We have obtained three long-slit, far UV spectra of the pre-main sequence system T Tauri. These HST/STIS spectra show a strong and variable on-source spectrum composed of both fluoresced H_2 and stellar chromospheric lines. Extended H_2 emission is seen up to $10''$ from the T Tau system. The on-source and extended H_2 are both pumped by H I Lyman α. The on-source H_2 is pumped by the red wing of a broad, self-absorbed Ly α line, while the progressions seen in the extended gas are pumped from near line center. This suggests that the extended H_2 is pumped locally, and not by the stellar Ly α line. The H_2 to the north and west coincides with the evacuated cavity bounded by the optical reflection nebulosity; to the south the extended H_2 coincides with the HH 255 outflow from the embedded infrared companion T Tau S. The spatial profile of the extended gas shows a prominent dip coincident with the position of T Tau S. This may be absorption by a disk associated with T Tau S. There is no evidence for absorption by a disk surrounding T Tau N large enough to obscure T Tau S.

Subject headings: stars: individual (T Tau), ISM: molecules

1. Introduction

Recent imaging and spatially-resolved spectroscopic observations of classical T Tauri stars and their environs show a bewildering variety of structures, from reflection nebulosities (e.g., McCaughrean & O'Dell 1996) to rings (e.g., Silber et al. 2000) and edge-on disks (e.g., McCaughrean et al. 1998). Some of this gas and dust represents the remnants of the birth cloud; some is in an infalling envelope; some is in the circumstellar disk (e.g., Adams, Lada, & Shu 1988). These stars often have collimated bipolar outflows orthogonal to the disks, with entrained Herbig-Haro nebulosities, as well as larger scale molecular outflows. The spatial scales range from a few stellar radii to thousands of astronomical units (AU).

The interactions between the circumstellar disk, the star, and the outflows play a central role in the late stages of star formation. The processes that clear away circumstellar disks are still not well quantified. However, our understanding of disk dispersal will certainly

be aided by any new information concerning the size and structure of gas disks and how central clearings and gaps develop within disks. In addition, observations of disk material in multiple star systems are relevant for the process of planet formation; Quintana et al. (2002) have shown that if planetesimals and planetary embryos form within disks in binary star systems, these bodies can subsequently accrete into terrestrial planets similar to those seen within our own Solar System. The spatial distribution of the molecular hydrogen (H_2) gas around classical T Tauri stars provides important information that can address these basic questions.

Spatially extended H_2 emission is common in the vicinity of young low mass pre-main-sequence (PMS) stars. This molecular emission is an important tracer of dynamical processes and shocks close to the PMS star. Most studies published to date have concentrated on the H_2 emission in the near-IR. Despite its abundance, H_2 is difficult to detect from the ground because the IR vibrational lines are forbidden quadrupole transitions and hence are weak. In contrast, the permitted UV Lyman band transitions are bright and dominate the far UV emission from many classical T Tauri stars when observed through large apertures (Valenti, Johns-Krull, & Linsky 2000). H_2 also dominates the far UV emission observed from low-excitation Herbig-Haro objects (e.g., Curiel et al. 1995).

H_2 is the major constituent of any cool gas. The astrophysics of H_2 has been reviewed by Field, Sommerville, & Dressler (1966) and by Shull & Beckwith (1982). Unlike CO, it does not readily deplete onto dust and, thus, persists in even the densest disk environments. H_2 is stable enough to resist dissociation even at temperatures of 2-3 $\times$ 10^3 K. H_2 is a homonuclear diatomic molecule; therefore, vibrational transitions within the $X^1\Sigma_g^+$ ground electronic level, falling in the near-IR, are forbidden. However, transitions between $X^1\Sigma_g^+$ and the $B^1\Sigma_u^+$ and $C^1\Pi_u$ electronic levels are permitted, resulting, respectively, in the Lyman and Werner bands. Emission in the Lyman bands lies shortward of 1700 Å. The HST can observe many of the Lyman band lines, while the Werner bands fall below 1200 Å. The upper levels of the UV lines have lifetimes of 10^{-8} s, compared with the 10^6 s lifetime of the IR transitions. Also the stellar photospheric continuum is much weaker at these wavelengths, allowing far easier detection of the H_2 emitting gas.

Valenti et al. (2000) detected H_2 emission from 13 of the 32 T Tauri stars observed at low (R$\sim$200) spectral resolution with the IUE. These Lyman band H_2 emission lines are fluorescently excited by the hydrogen Lyman α line at 1215.67 Å (Brown et al. 1981) and the molecular gas must be heated to $\sim$ 2000 K for the fluorescence to operate (Brown et al. 1981; Herbst et al. 1996). The heating is likely a result of shocks, but X-ray heating may also contribute (e.g., Lepp & McCray 1983; Maloney et al. 1996, Tine et al. 1997), especially very near the star. Ardila et al. (2002a) report on the H_2 emission observed in

8 classical T Tauri stars, as observed through the $2'' \times 2''$ aperture of the HST/GHRS. The H_2 emission is fluorescently pumped by the red wing of the stellar H I Ly α emission line. The lines are narrow, single-peaked, and optically thin. The lines may be blueshifted with respect to the stars, suggesting formation in an outflowing wind rather than in a rotating disk. The distribution of H_2 excitation temperatures appears to be non-thermal, suggesting shock excitation of the H_2 into the $X^1\Sigma_g^+$ state. Herczeg et al. (2002) determined that the on-source H_2 fluorescence in the UV spectrum of TW Hya is produced in or near the surface of the circumstellar disk.

1.1. T Tau

Our target was T Tauri (HD 284419), a system that has grown more and more complex as observations improve. The optically-visible northern component (T Tau N) is a classical T Tauri star, with evidence for on-going accretion. The canonical distance, which we adopt, is 140 pc. This is consistent with the Hipparcos parallax of 5.66±1.58 mas (ESA 1997). The star is oriented close to pole-on. The star has a 2.8 day rotation period (Herbst et al. 1986) and a rotational velocity v sin i of 20.1 km s^{-1} (Hartmann et al. 1986). Herbst et al. (1986) estimated an inclination i between 8 and 13°. Using a different estimate of the stellar radius, Herbst, Robberto, & Beckwith (1997) estimated i=19° (although they fixed i=10° for their disk modelling); Eislöffel & Mundt (1998) used the observed motions of the Herbig-Haro flow HH 155 (32″ west of T Tau N) to derive i=23°. T Tau N is detected at wavelengths from X-rays through the radio; the visual extinction A_V is estimated to be 1.4-1.5 mag (Cohen & Kuhi 1979, Kenyon & Hartmann 1995, Koresko, Herbst, & Lienert 1997, White & Ghez 2001). The broadband optical and near-IR fluxes of T Tau N have been fairly steady over the past half-century (Beck & Simon 2001). T Tau N has an optically thick dust disk spatially resolved at 3 mm (Akeson, Koerner, & Jensen 1998), with an ∼40 AU radius. Hogerheijde et al. (1997) found a disk radius <70 AU at 267 Ghz (1.1 mm).

Dyck, Simon, & Zuckerman (1982) showed that some of the near-IR excess arises in the southern component (T Tau S). T Tau S is the prototypical infrared companion (IRC), deeply embedded (A_V ∼35 mag; Koresko et al. 1997), and only visible in the IR, sub-mm and radio. T Tau S dominates the flux from the system in the mid- to far-IR. It does not appear to be extended in mm and sub-mm maps, and indeed was not detected by Hogerheijde et al. (1997) or Akeson et al. (1998), but the continuum variability and apparently non-thermal processes argue for significant ongoing accretion. Proposed causes for the high extinction include viewing T Tau S through an edge-on disk, or viewing a background T Tau S through the foreground face-on disk of T Tau N. Solf & Böhm (1999) argue that the outflows associated

with T Tau S are inclined by only about 11° to the plane of the sky, which supports the notion that T Tau S is viewed through a nearly edge-on disk.

The T Tau N-S binary separation is 0.70″ at a position angle of 180° (Duchêne, Ghez, & McCabe 2002). Roddier et al. (2000) show a change in position angle of about 0.66° yr^{-1}. It is likely that the N-S pair is a physical binary. Both stars drive bipolar outflows, leading to the complex velocity patterns seen in optical spectra, and powerful radio emission from the inner flow regions (Skinner & Brown 1994; Ray et al. 1997). Akeson et al. (1998) speculate that the circumstellar dust disk surrounding T Tau N may be tidally truncated by interactions with T Tau S. Following Hogerheijde et al. (1997), Solf & Bohm (1999) present a picture where T Tau S is viewed through an extended disk or envelope surrounding T Tau N.

Koresko (2000) and Duchêne et al. (2002) resolved T Tau S into T Tau Sa and T Tau Sb, with a separation of about 0.09″ in 2002. T Tau Sb appears to be a "normal" active low mass PMS star, with $A_V > 8$ mag. It cannot be buried within the same material obscuring T Tau Sa. Johnston et al. (2003) claimed that T Tau Sb is the T Tau S radio source, and that its motions relative to T Tau Sa are consistent with a highly eccentric (e=0.7), ≈40 year period orbit. The orbit does not appear to be coaligned with the jet axis. Loinard, Rodríguez, & Rodríquez (2003), accounting for the orbital motion of T Tau S, suggested that T Tau Sb is now moving linearly, having been ejected from the system during the past few years. Tidal truncation by this close companion may explain the absence of a spatially extended disk associated with T Tau S. Recently, Furlan et al. (2003) have muddied the situation by asserting that the system is at last quadruple. Their observations show that the T Tau S radio source and T Tau Sb are not the same, and they suggest that a close encounter between T Tau Sb and the radio source has ejected the latter.

The WFPC2 optical images (Stapelfeldt et al. 1998) show a reflection nebulosity extending ∼6″ in the N-S direction. The scattered light from the bright optical star prevented them from detecting reflection from a dust disk in the optical.

T Tau is by far the most extended and complicated PMS H_2 source in the near-IR (van Langevelde et al. 1994). Herbst et al. (1996) conducted K and H band imaging spectroscopy with a resolution of 0.7″ and detected up to 11 quadrupole H_2 lines in their brightest knots. Herbst et al. (1997), using Fabry-Perot imaging, recognized the presence of "a complex system of interlocking loops and arcs within 15″ of the central stars" and estimated a mass of 10^{-6} $M_\odot$ for the H_2 surrounding T Tau. Brown et al. (1981) showed that the Lyman band H_2 emission lines were spatially extended within the 10″×20″ large aperture of the IUE. This was confirmed by Walter & Liu (1997; see also Valenti et al. 2000), using HST observations of T Tau through the Large (2″) and Small (0.2″) apertures on the GHRS instrument.

Here we report on far UV long-slit observations obtained with the HST/STIS in an attempt to ascertain the origin of this extended emission in the T Tauri system.

2. HST Spectral Observations

We obtained four spectra of T Tau using the Space Telescope Imaging Spectrograph (STIS) on the Hubble Space Telescope as part of program 8157. Target acquisitions were made using the CCD, through the ND3 neutral density filter. The spectroscopic apertures are centered on T Tau N, the visible star. This paper concentrates on analysis of the three long-slit spectra that we obtained through the $0.2''$ slit. The long-slit covers $26''$ at a spatial scale of $0.0244''$ per pixel (3.4 AU per pixel). The 50% energy radius in the spatial profile is about 2.5 pixels ($0.06''$); a Gaussian fit to a stellar point spread function (PSF) summed from 1250 to 1700 Å gives σ=3.6 pixels ($0.09''$). At the nominal 140 pc distance of T Tau, the slit width is 28 AU. We did not search for spatial or velocity structures across the slit. The G140L grating provides a spectral resolution of about 2000 for a point source; our spectral resolution for any spatially extended emission is about a factor of 5 lower.

Although it is not important for spectra at this resolution, we have adopted a heliocentric radial velocity of 19 km s^{-1} for T Tau N (Hartmann et al. 1986). This is consistent with the 17.5 km s^{-1} we obtained from spectra taken with the Nordic Optical Telescope (NOT). We find a v sin i=20 km s^{-1} in the NOT spectra, in good agreement with Hartmann et al. (1986)[1].

The medium resolution (R=45000) E140M echelle spectrum was obtained through the $0.2{\times}0.06''$ (28×8.4 AU) aperture. This area is comparable to that contained in a 2 spatial pixel resolution element in the long-slit spectra. We concentrate here on the low dispersion spectra and use the high dispersion spectrum mainly for comparison and line identifications. Full analysis of the E140M spectrum will appear later.

The observing log is presented in Table 1.

Recently, Saucedo et al. (2003) have reported on analysis of an independent far UV long-slit observation of T Tau. They used a wider $2''$ slit, and consequently have lower spectral resolution and could not resolve the H_2 lines as well as we do. They observed at a different position angle (30°).

[1]We also obtained a high dispersion optical spectrum using the Kitt Peak National Observatory 4m echelle on 24 January 1997, using the standard red long setup and the T2KB CCD for a resolution of ≈50,000.

3. Overview of the Long-Slit Spectra

We obtained the long-slit spectra at position angles of 345, 10, and 100 degrees. Figures 1 and 2 show two of these spatially-resolved spectra. Figure 1, with the slit at a a position angle of 345°, shows the spatially-resolved spectrum corresponding to the NW-SE jet seen in the near-IR H_2 images (Herbst et al. 1996), and the bright extended emission in optical forbidden lines such as [S II] (Solf & Böhm 1999). This position angle corresponds to the outflow from T Tau S. Bright Lyman band H_2 emission is visible to 2-3″ either side of the star and fainter emission extends to greater distances to the south. The spatial distribution of H_2 at a position angle of 10° (not shown) is very similar. In the image at a position angle of 100° (Fig. 2) the H_2 is significantly less extended. This position angle corresponds to the outflows from T Tau N.

3.1. The On-source Spectrum

The on-source spectrum samples an approximately 24 AU × 28 AU region centered on T Tau N. The strongest lines in the on-source spectrum (Figure 3) are those of C IV, Si IV, and He II, powered by the accretion flow, the cooler O I lines from the stellar wind, and H_2 lines. A list of the strongest lines, with likely identifications, is provided in Table 2. The most pronounced difference from typical chromospheric spectra is the presence of many Lyman band H_2 lines photoexcited by Ly α throughout the spectrum. Identification of emission features requires an understanding of the expected H_2 emission spectrum because the H_2 emission lines are blended with the transition region, chromospheric, and wind lines, and are often blended with each other.

We predicted the H_2 lines from the on-source spectrum by calculating the H_2 emission for assumed Ly α profiles. This method is similar to the method Wood, Karovska, & Raymond (2002) used to analyse H_2 fluorescence from the wind of Mira B, although with their high-resolution spectra they could calculate a Ly α profile with resolved H_2 emission lines, while we assume a Ly α profile from which we calculate the H_2 emission. We fit the calculated H_2 emission to the spectrum by normalizing to the mean of the strongest H_2 lines in the spectrum that occur between 1430-1540 Å. The H_2 lines below 1400 Å tend to be weaker than expected from pure branching ratios calculated by Abgrall et al. (1993), due to a combination of extinction and optical depth effects. Because the lower levels of the short wavelength transitions have small energies, the opacity in these lower levels can be sufficient to weaken the flux in those transitions. We use an extinction of $A_V = 0.3$ (see §3.3) and then correct for the optical depth effects by fitting the H_2 lines at short wavelengths. Given the degeneracy between these effects, the precise value of the extinction used, even up to

$A_V = 1.5$, does not significantly change the calculated H_2 spectrum.

Many different Ly α emission profiles can reproduce the H_2 spectrum. However, we can constrain the Ly α profile given the relative flux from different fluorescent progressions. The resulting H_2 spectra are robust to the different acceptable Ly α profiles. Certain H_2 lines, most notably the 0-3 P(2) line at 1279.5 Å and a blend of lines at 1274 Å, are weaker than predicted by these models, which indicates possible problems with the calculated H_2 spectrum. However, we consider the model acceptable for our purposes here because the calculated H_2 spectrum resembles many detected features across the G140L bandpass.

In the CTTS, the strongest H_2 progressions are those pumped by the red wing of Ly α (Ardila et al. 2002a, Herczeg et al. 2002). This is also true of pattern of fluorescence in the on-source spectrum of T Tau. The strongest on-source H_2 emission lines have upper levels $v' = 0, J' = 1$, pumped at 1217.205 Å, $v' = 0, J' = 2$, pumped at 1217.643 Å, and $v' = 1, J' = 12$, pumped at 1217.904 Å. Emission from $v' = 1, J' = 4$, pumped at 1216.070 Å, is detected but weak, and emission from $v' = 2, J' = 5$, pumped by 1-2 R(6) at 1215.726 Å, is undetected. We detect no lines pumped from wavelengths shortward of the rest wavelength of Ly α. The progressions that we detect are summarized in Table 3.

It is possible to explain the weak flux in progressions pumped near line center of Lyman α if the H_2 sees a redshifted Lyman α profile from downflowing accreting material with a velocity >500 km s^{-1}. We consider such a large velocity unlikely, since it exceeds the free-fall velocity. Also, the strong accretion lines unaffected by wind absorption (S III, S IV, C IV, He II, and Cl I λ1351) are not redshifted in the high dispersion spectrum. Self-absorption in the Lyman α line is likely to explain the observed pattern of H_2 emission, if the H_2 lies outside the wind acceleration region. The strong O I and C II lines in the 1300-1340 Å region are strongly self-absorbed by the stellar wind, with no emission blueward of line center. Similar absorption likely exists in the Ly-α line. Unlike the case of some other T Tauri stars, the wind velocity of T Tau N is not sufficient to absorb any strong predicted H_2 lines, so we cannot determine where the on-source H_2 is formed relative to the stellar wind. Our modelling of the Lyman α line profile seems to suggest a need for a modest redshift of the emission centroid in addition to self-absorption.

After identifying the likely H_2 lines, we can identify other strong emission features that are most likely produced in the accretion shock or the wind. The strongest emission lines are the partially resolved C IV doublet at 1550 Å and He II emission at 1640 Å. The emission at 1393 Å and 1402 Å, identified in cool stars as Si IV emission, is a blend of Si IV and H_2 emission. Similarly, emission at 1335 Å is a blend of C II and H_2 emission.

Emission at 1238 Å, which could in principle be H_2 emission, is more likely N V emission,

although the N V 1243 Å line is not present. Wilkinson et al. (2002) detected O VI emission at 1032 Å[2], so we expect the accretion shock to be hot enough to excite N V emission. A possible explanation for the absence of the 1243 Å line is absorption by a complex of four excited N I lines, about 2.4 eV above the ground state. A blueshift of about 100 km s^{-1}, consistent with a stellar wind, is needed to blanket the N V 1243 Å line.

The CO A $^1\Pi - X\ ^1\Sigma^+$ line system lies between 1540 and 1970 Å. These lines are photoexcited by the strong Si IV and C IV accretion lines. We looked for these lines, but saw no evidence of any CO emission. This is not surprising: the abundance of CO, even assuming no depletion of the CO, is about 10^{-4} that of H_2.

3.2. Variability in the On-source Spectrum

The stellar flux from T Tau varied between these observations. We compared the flux in the three long-slit spectra by extracting the spectrum within 3 spatial pixels of the peak pixel ($\pm 0.085''$); the total area in the extraction aperture is 0.024 square arcsec.

3.2.1. Lyman α emission

There is a variable emission line centered at 1220 Å (Figure 4), which we identify as the red wing of the stellar H I Ly α emission line. The line is not spatially extended; it is presumably dominated by emission from the accretion shock. From 2000 Nov 26 to Dec 1 the line strength increased proportionally with the other emission lines. It was absent a month later, and was also not seen in the E140M observation about 3 months previous. We conclude that the line is stellar because it is spatially coincident with the star in two observations with position angles differing by 125°, and the observed wavelength does not change. Were the source of the Ly α emission not coincident with T Tau N, and hence not centered within the aperture, it should be present in the other observation at a different spatial location.

The red edge of the Ly α emission line extends to about 1223Å. Assuming the line is symmetric and centered at the stellar rest velocity, the FWHM of the line corresponds to a velocity of 950 km s^{-1}. Such a broad Ly α emission line is not unprecedented; HST/STIS spectra of RU Lupi and DF Tau show red emission wings at about $\lambda\lambda$1218-1222 Å. The

---

[2]The 1038 Å O VI line is absorbed by cold H_2 from v''=0, J=0,1,2 lower levels. This H_2 is much colder than the gas we see emitting here.

unusually unobscured, pole-on star TW Hya shows a broad Ly α emission profile extending about 4 Å both to the blue and red of line center (Herczeg et al. 2002). For comparison, the FWHM of the Mg II k & h lines is about 225 km s^{-1} (Ardila et al. 2002b), the FWHM of the Si IV λ 1393Å and C IV λ 1551Å lines in the high dispersion spectrum is about 200 km s^{-1}, and the FWHM of the H α line in our KPNO echelle spectrum is 250 km s^{-1}.

The line profiles seen on 2000 Nov 26 and Dec 1 are similar, with peak flux near 1220 Å. This suggests that it is the intrinsic line strength, and not the extinction, which is changing. A simple model of a Gaussian line with variable line strength and fixed σ=3.3 Å absorbed by n_H=4.0×10^{20} cm^{-2} reproduces the observed profiles (see §3.3).

The H_2 emission is photoexcited by Ly α and can therefore be used as a proxy for Ly α emission. The H_2 emission on December 1 is about 60% stronger than on November 26, which in turn was about 10% stronger than on January 5. The sense of the variations agrees with the observed red wing flux of Ly α. The relative H_2 emission line strengths show no significant differences between the 3 observations.

3.2.2. The Accretion Continuum

Figure 5 shows the ratio of the flux on 2000 Dec 1 to those on the 2000 Nov 26 and 2001 Jan 5. The mean flux level is about 30% higher on Dec 1. The excess flux is blue, and is not detected longward of about 1650 Å, where the true stellar photospheric continuum begins to become detectable, suggesting possible excess accretion heating as the source. This is corroborated by the behavior of the fluxes in the strong lines. The H I Ly α emission is strongest on Dec 1 (see §3.2.1). The fluxes in the strong C II, Si IV, and C IV lines are enhanced by about a factor of 2 on Dec 1, while the cool wind lines (O I and the $\lambda\lambda$1350 and 1670 Å complexes) appear to be depressed on Dec 1. This increase in emission line strengths due to enhanced accretion heating is a specific example of the general case that the PMS stars with the largest accretion rates also have the strongest emission lines (e.g., Johns-Krull, Valenti, & Linsky 2000).

The mean continuum flux on Nov 26 was 1.06 times that on Jan 5. We conclude that the accretion rate was enhanced on or about Dec 1, which increased the accretion continuum brightness by about 30% while increasing the accretion heated lines by a larger factor and suppressing the emission from the cool wind. The presence of H I Ly α emission on Nov 26 suggests that the accretion episode may have been starting about then, and was over within a month.

3.3. The Extinction

The canonical visual extinction A_V for T Tau N is 1.5 mag. However, we believe that the true extinction column is significantly smaller than implied by this A_V.

Based on the spectral lines in the λ6495 Å region (from optical echelle spectra obtained using KPNO 4m telescope), we concur with Cohen & Kuhi (1979) that the spectral type is K1 IV, with an uncertainly of about 1 spectral subtype (other authors, such as Bertout, Basri, & Bouvier (1988) and White & Ghez (2001), assign a K0 spectral type). Interpolating between the colors for giants and dwarfs, we expect the intrinsic $V - I_c$ color of a K1 subgiant to be about 1.0 (colors are 0.93 and 1.08 for luminosity classes V and III, respectively). The $V - I_c$ color of 1.45 gives a color excess of 0.45 mag. The standard reddening vector (with the ratio of total to selective absorption R_V=3.1) then implies A_V=1.2 mag. A $\pm$1 spectral subtype uncertainty corresponds to an uncertainty in A_V of 0.2 mag; uncertainty in the exact intrinsic color of a K1 IV star corresponds to an uncertainty in A_V of up to 0.3 mag, in the sense that a star with surface gravity and colors closer to a giant than a dwarf has a smaller extinction. The canonical A_V=1.5 mag can be reproduced by assuming dwarf colors for unreddened photosphere. If any of the near-IR excess spills over into the I band the extinction will be overestimated.

We measured the X-ray absorption N_X by fitting the ROSAT PSPC spectrum of T Tau with a two-component thermal model. The best fit X-ray absorption is 3.0×10^{21} cm^{-2}, which corresponds to A_V=1.7 mag. However, the uncertainty on the extinction is consistent with A_V=0 at 1σ.

We can use information from the UV spectra, where the opacity is larger and the effects of extinction more extreme, to check the optical extinction.

We estimate the H I absorption column directly from the shape of the Ly α profile (§ 3.2.1). We assume a symmetric Gaussian emission line centered at the stellar radial velocity and self-absorbed on the blue side. The red wing (longward of 1220 Å in the December 1 spectrum) constrains the line width; we find that the Gaussian σ=3.3 Å (FWHM=3.9 Å). The width of the central line reversal then sets the absorption column to be $n_H=4\times10^{20}$ cm^{-2}, which corresponds to A_V of about 0.2 mag, for a normal gas-to-dust ratio and R_V=3.1. This extinction is significantly smaller than the canonical value. However, if the absorbing gas is blueshifted with respect to the Ly α emission, this technique will underestimate the absorption column. An absorption column of $n_H=3\times10^{21}$ cm^{-2} corresponding to the optical extinction can match the observed profile for blueshifted absorption velocities of $\sim$1000 km s^{-1}. This is unlikely, not only because the high required velocity exceeds that of the winds of other PMS stars, but also because there would then be significant absorption of the Si III λ1206Å

line by the blueshifted gas.

The ratio of C III λ1175 to C III λ977 fluxes provides another constraint on A_V, so we examined the FUSE spectrum of T Tau (Wilkinson et al. 2002). In the high density limit ($n_e > 10^{10}$ cm^{-3}), which seems reasonable for an accretion shock, we expect an intrinsic C III λ1175/C III λ977 flux ratio near 0.6 (e.g., the CHIANTI database; Dere et al. 1997). We observe a flux ratio of about 1.44 (averaging the fluxes from each of the two FUSE detectors). For R_V = 3.1, this suggests n_H=7$\times$10^{20} cm^{-2}. However, this line ratio is not conclusive because the C III λ1175 Å lines are contaminated by H_2 Werner band emission and the C III λ977 Å line may suffer absorption from Werner band lines arising from ν''=0, and because there is likely wind absorption in the C III λ 977 Å line. Allowing for a factor of two uncertainty in the true line ratio, the allowable column for R_V = 3.1 ranges from 2$-$12$\times$10^{20} cm^{-2}. This is consistent with the Ly α column, but not with the optical extinction, which corresponds to n_H=2.2$\times$10^{21} cm^{-2}.

We note that TW Hya, a system with A_V $\sim$0, has very nearly the same C III λ1175/C III λ977 ratio (1.41). On the assumption that TW Hya and T Tau N, both face-on accreting systems, have intrinsically similar spectra and wind absorption, then the similar line ratios suggests similar, and small, values of the ultraviolet extinction.

The discrepancy between the optical column implied by A_V and that in the ultraviolet suggests at least three possible solutions. The first is that the extinction to the site of the formation of the Ly α and C III lines is less than that to the photosphere. The second is that R_V may be larger than the standard value of 3.1. The third is that the colors do not accurately reflect the intrinsic spectral type.

While one could imagine a geometry that would lead to significantly inhomogeneous extinction near the star, we do not consider the first possibility further.

R_V is often larger than the standard value of 3.1 in star forming regions, possibly due to the presence of large grains. We used the Cardelli et al. (1989) parameterization of the extinction laws to search for a value of R_V that would self-consistently agree with the optical and UV extinctions. While a wavelength of 977 Å is below the formal 1000 Å limit of their parameterization, the extrapolation to 977 Å is not inconsistent with FUSE reddening results (Hutchings & Giasson 2001). Adjusting R_V affects the relative extinctions of the C III lines and the inferred optical column, but it does not alter the Ly α column, which is a direct measurement of the H I column. We find that the optical and C III absorption columns agree, at n_H $\sim$1.3$\times$10^{21} cm^{-2}, for R_V $\sim$5. This column is still about 3 times that directly measured at Ly α.

Why does the optical color excess imply a much larger extinction? Intrinsic photospheric

colors generally pertain to ideal stars with uniform surface temperatures. Gullbring et al. (1998) show that weak-lined T Tauri stars have $V - I$ colors up to 0.2 mag redder than main sequence stars of the same spectral type. They show that this could plausibly be due to a large filling factor (up to 70%) of cool starspots. While their investigation is specific to cooler (K7-M1) stars, the effect is presumably still evident in spotted K1 stars. This effect could account for up to nearly half the observed $V - I$ color excess.

Finally, the foreground extinction can be estimated from observations of objects that are spatially proximate to T Tau. Cardelli & Brugel (1988) found the extinction to HH 255 (Burnham's Nebula) to lie between A_V=0.24 (R_V ∼5) and A_V=0.34 (R_V=3.2). HH 255 is the outflow from T Tau S; this extinction measures a line of sight <10″ from that to T Tau N. Unless there is a very large circumstellar contribution to the T Tau N extinction (T Tau N is viewed nearly pole-on, where circumstellar extinction should be minimized), then the extinction to T Tau N may be similarly small.

The small extinction to HH 255 and the UV diagnostics suggest that the ultraviolet extinction is indeed much less than expected for A_V=1.5 mag. On these grounds we justify our use of $n_H=6\times10^{20}$ cm^{-2} for modelling the H_2 line spectrum.

3.4. The Off-source Spectra

The spatial structure of the H_2 emission lines provides us with a variety of regions from which we can extract spatially-resolved spectra. The emission strength decreases with distance from T Tau N. The strongest discrete feature lies between 1″ and 2″ south of T Tau N, and is seen in the images at 345° and 10° position angles. We call this the Southern Knot. The weaker emission south of that, from 2″ to 9″ south of T Tau N, is the Faint Southern Extension (FSE). Similarly, the weak emission west of T Tau N at position angle 100° is the Faint Western Extension (FWE). We extracted spectra from these regions and compared them to each other and to the on-source spectrum.

The spectra seen in the FSE, FWE, and the Southern Knot are all similar to each other (see Figure 6). The *only* detected H_2 lines are pumped by 1-2 R(6) at 1215.726 Å and 1-2 P(5) at 1216.070 Å, 12 and 96 km s^{-1}, respectively, redward of the center of the Ly α line. These progressions are the most prominent H_2 lines in sunspots (Jordan et al. 1978) and in low-excitation H-H objects (Curiel et al. 1995; Schwartz 1983; Schwartz, Dopita, & Cohen 1985). The flux ratio of the two progressions are similar for each of the different regions studied. The H_2 lines below 1300 Å are weaker, relative to lines above 1400 Å, in the Southern Knot than in the other regions, either due to higher extinction towards the knot

or a larger optical depth of H_2.

There appears to be continuum emission between the H_2 lines. We have neither the spectral resolution not the S/N to determine whether this is a H I 2-photon continuum, or an H_2 continuum. It is most likely not a reflection of T Tau N, in which case the strong transition region and wind lines should dominate.

This H_2 spectrum contrasts strongly with that seen on-source (§3.1). The off-source H_2 cannot be pumped by the same source that pumps the on-source H_2; the off-source H_2 sees a narrow unabsorbed Ly α profile. This conclusion differs from that of Saucedo et al. (2003), who conclude that the FWE emission and the emission to the north of T Tau N are pumped by stellar Ly α from T Tau N.

The exact spatial regions in the FSE and the Southern Knot sampled in the two N-S observations are not identical due to the 25° difference in the slit position angle. The H_2 emission detected in the FSE has the same strength in both observations, but the continuum is 20% stronger on December 1. The continuum in the Southern Knot has the same strength in both observations, but the H_2 emission was about 20% brighter on December 1 than on January 5.

4. The Spatial Profile of the Emission

The long-slit spectra encompass the geocoronal H I Ly α and O I λ1304 Å lines. It is evident in Figures 1 and 2 that they extend the full length of the slit. Aside from a systematic 5% decrease in the mean flux level from the bottom to the top of the PA=10° image, there are no significant spatial variations in the flux of the geocoronal lines. The distribution of flux values is consistent with a Gaussian with σ=0.04 of the mean. We take this to indicate that the MAMA detector is flat-fielded to about 4%, and that any spatial variations greater than this are unlikely to be instrumental.

The spatial profile of the extended emission about T Tau is highly structured. In order to examine the spatial structure on the smaller scales of interest, the sizes of the disk and the separation between then components, it is necessary to separate out the stellar point spread profile. For a reference point spread profile we use a STIS spectrum of the UV-bright polar AR UMa (observation o53y01020), observed with the identical instrumental setup. We aligned the spatial profiles by centroiding on the seven central pixels. The profiles are normalized such that they have the same median background level far from the source, and a maximum of one.

We examined the PSF for three spectral regions: the prominent H_2 lines in the spectrum of the Southern Knot (Table 4), the prominent stellar lines listed in Table 5 (some of which are contaminated with H_2 emission), and some regions between the lines that we call continuum (Table 5), but which may have a large contribution of weak line flux. In an attempt to clearly separate the components, we have avoided the λ1547 Å line, the strongest in the stellar spectrum, since it is a combination of presumably stellar C IV (seen on-source) and the H_2 R(3) 1→8 H_2 line, which is seen off-source. Similarly we have avoided the lines at $\lambda\lambda$1239 Å, 1465 Å, 1505 Å, and 1602 Å, which have both stellar atmospheric and extended H_2 lines at similar wavelengths.

In the two observations with the generally north-south orientation, the bright southern knot at $-1.3''$ dominates the extended emission, separated from the star by a prominent dip at $-0.7''$ (Figure 7). This dip coincides with the location of T Tau S. The enhanced H_2 flux extends from about $-1.7''$ to about $+0.6''$. The extended emission falls off to about $2.5''$ north, while to the south the emission plateaus at a lower level between $-5''$ and $-2.5''$, and reappears at a similar level between $-9''$ and $-7''$.

We examined the inner $0.2''$ of the spatial profiles for evidence of spatial extent. This region is shown in Figure 8. For the H_2, an appropriate reference profile is the point source profile superposed on an enhanced background, on the assumption that the extended emission is continuous across the position of the star. Both the H_2 and stellar line profiles appear to be slightly extended with respect to the reference profile. Deconvolution of the reference profiles yields H_2 source widths ranging from about 1 pixel (2.8 AU) at about 80% of the peak flux to 8 pixels (28 AU) at 10% of the peak flux. This may be evidence for a brightening of the background close to the star, perhaps associated with the disk around T Tau N.

The stellar profile is always less extended than the H_2 profile, but shows the same overall shape. We ascribe this to weak H_2 emission lines contaminating the stellar profile.

Figure 9 shows the east-west profile. Weak emission is clearly seen to the west in H_2, extending out about $12''$. Any spatial extent to the east is small. The extent seen in the inner $0.15''$ is similar to that seen in the north-south profile. There is no discernable extent to the stellar line profile.

4.1. Modelling of the Spatial Profile

Our three spatial cuts are clearly not sufficient to construct a detailed map of the spatial distribution, but they let us examine some very simple models for the origin of the fluorescent off-source H_2 emission. The H_2 could lie in a diffuse three-dimensional volume surrounding

the T Tau system, it could lie on the surface of a circumstellar disk, or, in the absence of a large optically thick disk around T Tau N, could lie on the surface of a nearby background molecular cloud.

We exclude the hypothesis that the emission arises on the surface of a large gaseous disk surrounding T Tau N, because the stellar rotational orientation suggests that any disk should be nearly face-on. If so, the extents seen in the N-S cuts should be mirrored in the E-W cuts.

The WFPC2 image (Stapelfeldt et al. 1998) appears to show optical reflection from the interior of a cavity evacuated by the wind of T Tau N. Our data are broadly consistent with this model. Since the spatially distributed H_2 lines are pumped from the center of a narrow Ly α line, we seem to need a spatially distributed pumping source. We should not assume that there is a single central pumping source, unlike in the case of the optical image where the reflection nebulosity is illuminated by the central star. The H_2 spatial intensity distribution is a convolution of the distribution of shocked gas with the H_2 gas density, modified by foreground extinction.

We generated a simple phenomenological model that reproduces the gross characteristics of the spatial profile within $2''$ of T Tau N (Figure 10). This model assumes a linear variation of the H_2 surface flux from the southern knot to the plateau to the north. To that we add a point source at the position of T Tau N and an absorption dip centered near the position of T Tau S. This is all then convolved with the point spread function.

The absorption dip is broad, with edges sharper than a simple Gaussian function. A rectangle with unresolved sides and a flat bottom, after convolution provides a satisfactory representation of the shape of the dip. The best-fit half width is $\pm 0.32''$. The flux at the bottom of the dip, prior to convolution with the point source profile, is about 15% of the interpolated flat model. We attempted to model the absorption using softer edges, such as a Gaussian profile, but these failed to reproduce the observed intensity profile. The requirement for a sharp-edged absorption is robust so long as the extended emission is reasonably smooth on spatial scales of an arcsecond or more, as appears to be the case. This requires that absorbing medium be foreground to 85% of the H_2 emission.

The dips visible in the two north-south orientations are similar but not identical. At the 345° position angle, we find that the absorption is centered about $-0.62''$, while at the 10° position angle the dip is centered at $-0.74''$. The uncertainties on the positions are hard to estimate, since the central position depends strongly on the gradient of the emission in this region. However, as is visible in Figure 11, the $0.1''$difference in offset is significant. The dip is also broader, by about $0.1''$, in the 10° position angle observation.

At a distance of 0.7″ from T Tau N, the two north-south orientations are separated by about 0.3″. They sample nearby, but independent, regions on the sky. The two dips are consistent with absorption by a foreground extended structure. The north-south thickness of the absorber is 0.64″; its length exceeds 0.5″. It is premature to deduce a shape for the absorber from these data, but we suggest that this structure may be the edge-on disk of T Tau S seen in absorption.

4.2. The Origin of the Extended H_2

As noted also by Saucedo et al. (2003), the distribution of H_2 emission revealed by our long-slit spectra has notable similarities to structure detected in prior optical observations. The WFPC2 optical images of Stapelfeldt et al. (1998) show a curved reflection nebulosity illuminated by T Tau N, extending ∼6″ in the N-S direction. The shape of the nebulosity is consistent with models of reflection from the interior of a cavity evacuated by the E-W stellar wind from T Tau N (Calvet et al. 1994). In the Stapelfelt et al. model the cavity is open to the west and inclined to the line of sight at an angle of $\sim 45°$. In Figure 12 we overlay our summed H_2 long-slit signal on the Stapelfeldt et al. contour plot. At least along the cuts we have sampled, the fluorescing H_2 appears to fill the volume that is foreground to the cavity wall responsible for the reflection nebulosity. To the north, east, and west the extent of the H_2 emission is bounded by the cavity structure.

The situation is more complicated to the south, where our bright Southern Knot and Faint Southern Extension emission lies well outside the structure responsible for the reflection nebulosity. These emissions clearly arise from a different structure, known as HH 255, that is seen in optical long-slit spectra (Solf & Böhm 1999; Matt & Böhm 2003) and is associated with the outflow from T Tau S. Structure in [S II] λ6731 emission correlates very well with that seen in H_2; in particular our Southern Knot corresponds to a region of strong [S II] that lies up-wind of a standing shock within the jet that forms due to the jet collimation process. The shock velocity is ∼90 km s^{-1} and results in temperature high enough to produce [O III] emission and destroy H_2. This shock region is seen as a steep edge in the H_2 emission located beyond −2.0″ in Figure 7. It is unclear whether the faint H_2 emission that extends far to the south of this shock is related to the jet outflow or some other diffuse gas. The [S II] $\lambda6731/\lambda6716$ ratio suggests that the electron density within our Faint Southern Extension is $\sim 1\times10^3$ cm^{-3} (Matt & Böhm 2003).

4.3. Implications for T Tau S

We speculate that the discrete dark feature at $-0.7''$ may be the shadow of the edge-on disk of T Tau S. This is suggested primarily by spatial coincidence. The shadow is dark; any foreground H_2 (or other far UV) flux contributes no more than about 15% of the interpolated background flux. Note that this absorber is detected only in the far UV, where the opacity is relatively large; the detection of absorbing matter in the far UV is not inconsistent with the failure to detect extended optically thick material at mm wavelengths.

If T Tau S has an extended disk, the 11° orientation of its rotation axis from the plane of the sky suggests that the disk should be seen close to edge-on, at a position angle close to perpendicular to the 345° position angle of the outflow from T Tau S. We note that any elongated structure at a position angle perpendicular to the T Tau S outflow will be seen offset from T Tau N by 0.67 and $0.75''$, respectively, in the 345° and 10° scans. This is consistent with the observed positions of the dips in the two scans.

Any disk is likely to be severely truncated by the presence of T Tau N and T Tau Sb. If T Tau S has a 40 AU ($0.28''$) radius disk like T Tau N, then the thickness of the disk must be about $0.2''$, a significant fraction of the radius, to account for the observed width of the absorption dips. We do not have the spatial coverage to constrain the spatial extent of the absorption along the major axis of the possible disk. We note that the inferred extent of the absorbing material is substantially larger than the inferred radius of the T Tau Sa/Sb orbit. Clearly, an image of this system in the light of the H_2 Lyman bands would greatly clarify matters.

The presence of an absorber associated with T Tau S suggests that T Tau S is not seen through the disk of T Tau N because then the disk of T Tau N should also cast a shadow. While we cannot unequivocally prove that there is extended emission between T Tau N and T Tau S, there is no comparable absorption dip to the north or east. If the dip is due to a disk surrounding T Tau N, it is a most unusually shaped disk.

If the absorption feature is a foreground structure around T Tau S, then we suggest that the strong variability of T Tau N, visible before about 1917 (Beck & Simon 2001), is attributable to the line of sight to T Tau N passing through thick material in the equatorial plane of T Tau S. Assuming the equatorial plane is perpendicular to the outflow direction, and assuming a 550 year circular orbit (Roddier et al. 2000) and no precession, then T Tau N would have been in the equatorial plane of T Tau S in about 1850, and perpendicular to the plane in about 1985. If there is a substantial amount of circumstellar material associated with T Tau S, we would expect it to have maximally obscured a background T Tau N around 1850. This is consistent with the Beck & Simon (2001) light curve, which shows

T Tau N uniformly faint from 1899 through 1902 (an admittedly short interval), and then highly variable until 1917. It is also consistent with the light curve of Lozinskii (1949), covering the interval 1858-1941. His light curve shows long intervals between 1858 and 1870 when T Tau N appeared to be very faint (magnitude $\sim$13, as opposed to $\sim$magnitude 10 after 1917). From 1902 to 1917 the projected perpendicular distance from T Tau N to the equatorial plane of T Tau S increased from about $0.45''$ to $0.53''$. This is somewhat larger than our inferred projected disk thickness of $0.32''$.

T Tau N appears not to be intrinsically highly variable: its photographic magnitude has been essentially constant since 1926. T Tau N will again lie in the equatorial plane of T Tau S in about the year 2175; if the orbit is coplanar with the disk of T Tau N (a dubious assumption given the absolute non-coaxiality elsewhere in the system), T Tau S is currently receding from us on its orbit, and will be in the background in 2175. We would expect that T Tau N will remain fairly bright for the next 325 years, and then will once again become a highly variable star.

5. Conclusions

T Tauri continues to confound and perplex, but better observational data are yielding new insights. This is a possibly heirarchical, but clearly a non-coaligned, system. The rotation (outflow) axes of T Tau N and T Tau S are nearly orthogonal. The Sa-Sb orbit appears not to lie in the equatorial plane of Sa. Understanding the orbits of and relative distances to these stars is important in the context of the formation of multiple stars.

The on- and off-source H_2 spectra are very different. The on-source H_2 is pumped by the red wing of the broad self-absorbed Ly α line produced by the accretion flow. By contrast, the spatially extended H_2 lines are pumped from near the center of the Ly α line. Since the broad stellar line is self-absorbed, the extended warm H_2 must be pumped from another source. A likely candidate is Ly α generated in the same shocks that heat the H_2 (e.g., Wolfire & Königl 1991). There are at least two stars producing voluminous outflows, including HH objects, in this system, so there is no lack of energy to drive the shocks.

The strong H_2 emission north and west of T Tau appears to trace gas within the west-facing cavity bounded by the bright reflection nebulosity in the WFPC2 image. The bright H_2 emission to the south coincides with the pre-shock HH 255 outflow from T Tau S. Future H_2 long-slit spectroscopy or imaging should be able to reveal the structure of the T Tau S disk and jet collimation region in considerable detail.

If the dip in the brightness profile is related to T Tau S, then T Tau S is in front of

85% of the fluorescing gas. It is probably not obscured by a large disk surrounding T Tau N. Rather, the irregular variability of T Tau N may be due to extinction by material associated with T Tau S. T Tau N may once again become a highly variable star in about the year 2325.

Reconstruction of the spatial distribution of the gas from the long-slit images tantalizes one with the wealth of information suggested. All the off-star emission shortward of 1700 Å is fluorescent H_2 Lyman band emission. A 1300-1700Å-band image with HST/ACS would directly reveal the location of the gas and the shocks. It would show the structure of the cavity, or of any other features, on spatial scales of about 4 AU. An image would show instantly whether or not the dark region is indeed the shadow of T Tau S, and give the size, shape, and orientation of this dark matter. The far UV offers a surprisingly clear view with which to penetrate the dusty veils of star formation.

We thank Tracy Beck for providing many insights into the T Tau system, as well as a critical reading of the manuscript. This research was funded in part by STScI grant GO-08157.01-97A to SUNY Stony Brook, by STScI grant GO-08157.02-97B to the University of Colorado, and by the Swedish National Space Board.

This paper is based on observations made with the NASA/ESA Hubble Space Telescope, obtained at the Space Telescope Science Institute, which is operated by the Association of Universities for Research in Astronomy, Inc., under NASA contract NAS 5-26555. These observations are associated with program 8157.

REFERENCES

Abgrall, H., Roueff, E., Launay, F., Roncin, J.-Y., & Subtil, J.-L. 1993, A&AS, 101, 273

Adams, F.C., Lada, C.J., & Shu, F.H. 1988, ApJ, 326, 865

Akeson, R.L., Koerner, D.W. & Jensen, E.L.N., 1998, ApJ, 505, 358

Ardila, D.R., Basri, G., Walter, F.M., Valenti, J.A., & Johns-Krull, C.M., 2002, ApJ, 566, 1100

Ardila, D.R., Basri, G., Walter, F.M., Valenti, J.A., & Johns-Krull, C.M., 2002, ApJ, 567, 1013

Beck, T.L. & Simon, M. 2001, AJ, 122, 413

Bertout, C., Basri, G., & Bouvier, J. 2001, ApJ, 330, 350

Brown, A., Jordan, C., Millar, T.J., Gondhalekar, P., & Wilson, R. 1981, Nature, 290, 34

Calvet, N., Hartmann, L., Kenyon, S.J., & Whitney, B.A. 1994, ApJ, 434, 330

Cardelli, J.A. & Brugel, E.W. 1988, AJ, 96, 673

Cardelli, J.A., Clayton, G.C., & Mathis, J.S. 1989, ApJ, 345, 245

Cohen, M., & Kuhi, L.V. 1979, ApJS, 41, 743

Curiel, S., Raymond, J.C., Wolfire, M., Hartigan, P., Morse, J., Schwartz, R.D., & Nisenson, P., 1995, ApJ, 453, 322

Dere, K.P., Landi, E., Mason, H.E., Monsignori Fossi, B.C., & Young, P.R. 1997, A&AS, 125, 149

Duchêne, G., Ghez, A.M., & McCabe, C. 2002, ApJ, 568, 771

Dyck, H.M., Simon, M., & Zuckerman, B. 1982, ApJ, 255, L103

Eislöffel, J. & Mundt, R. 1998, AJ, 115, 1554

ESA. 1997, The Hipparcos and Tycho Catalogues (SP-1200) (Noordwijk: ESA)

Field, G.B., Sommerville, W.B., & Dressler, K. 1966, ARA&A, 4, 207

Furlan, E., Forrest, W.J., Watson, D.M., Uchida, K.I., Brandl, B.R., Keller, L.D., & Herter, T.L. 2003, astro-ph/0307355

Gullbring, E., Hartmann, L., Briceno, C., Calvet, N. & Muzerolle, J. 1998, in "The Tenth Cambridge Workshop on Cool Stars, Stellar Systems and the Sun", eds. R.A. Donahue & J.A. Bookbinder, ASP Conference Series #154, (San Francisco: ASP) p. 1709

Hartmann, L., Hewett, R., Stahler, S., & Mathieu, R.D. 1986, ApJ, 309, 275

Herbst, T.M., Beckwith, S.V.W., Glindemann, A., Tacconi-Garman, L.E., Kroker, H., & Krabbe, A. 1996, AJ, 111, 2403

Herbst, T.M., Robberto, M. & Beckwith, S.V.W. 1997, AJ, 114, 744

Herbst, W. et al. 1986, ApJ, 310, L71

Herczeg, G.J., Linsky, J.L., Valenti, J.A., Johns-Krull, C.M., & Wood, B.E., 2002, ApJ, 572, 310

Hogerheijde, M.R., van Langevelde, H.J., Mundy, L.G., Blake, G.A., & van Dishoeck, E.F. 1997, ApJ, 490, L99

Hutchings, J.B. & Giasson, J., 2001, PASP, 113, 1205

Johns-Krull, C.M., Valenti, J., & Linsky, J.L. 2000, ApJ, 539, 815

Johnston, K.J., Gaume, R.A., Fey, A.L., de Vegt, C., & Claussen, M.J. 2003, AJ, 125, 858

Jordan, C., Brueckner, G.E., Bartoe, J.-D.F., Sandlin, G.D., & VanHoosier, M.E. 1978, ApJ, 226, 687

Kenyon, S.J. & Hartmann, L. 1995, ApJS, 101, 117

Koresko, C.D. 2002, ApJ, 531, L147

Koresko, C.D., Herbst, T.M., & Lienert, Ch. 1997, ApJ, 480, 741

Lepp, S. & McCray, R. 1983, ApJ, 269, 560

Loinard, L. Rodríguez, L.F., & Rodríguez, M.I. 2003, ApJ, 587, L47

Lozinskii, A.M. 1949, Perem. Zvedzy, 7, 76

Maloney, P.R., Hollenbach, D.J. & Tielens, A.G.G.M. 1996, ApJ, 466, 561

Matt, S. & Böhm, K.-H. 2003, PASP, 115, 334

McCaughrean, M.J., Chen, H., Bally, J., Erickson, E., Thompson, R., Rieke, M., Schneider, G., Stolovy, S. & Young, E. 1998, ApJ, 492, L157

McCaughrean, M.J. & O'Dell, C.R. 1996, AJ, 111, 1977

Quintana, E.V., Lissauer, J.J., Chambers, J.E., & Duncan, M.J. 2002, ApJ, 576, 982

Ray, T.P., Muxlow, T.W.B., Axon, D.J., Brown, A., Corcoran, D., Dyson, J., & Mundt, R. 1997, Nature, 385, 415

Roddier, F., Roddier, C., Brandner, W., Charissoux, D., Véran, J.-P., & Courbin, F. 2000, in "Birth and Evolution of Binary Stars, Poster Proceedings of IAU Symposium No. 200 on The Formation of Binary Stars", Eds. B. Reipurth & H. Zinnecker, p. 60.

Saucedo, J., Calvet, N., Hartmann, L., & Raymond, J. 2003, ApJ, 591, 275

Schwartz, R.D. 1983, ApJ, 268, L37

Schwartz, R.D., Dopita, M.A., & Cohen, M. 1985, AJ, 90, 1820

Shull, J.M. & Beckwith, S. 1982, ARA&A, 20, 163

Silber, J., Gledhill, T., Duchêne, G., & Ménard, F. 2000, ApJ, 536, L89

Skinner S.L. & Brown, A. 1994, AJ, 107, 1461

Solf, J. & Böhm, K.-H. 1999, ApJ, 523, 709

Stapelfeldt, K.R. et al. 1998, ApJ, 508, 736

Tine, S., Lepp, S., Gredel, R., & Dalgarno, A. 1997, ApJ, 481, 282

Valenti, J., Johns-Krull, C.M., & Linsky, J.L. 2000, ApJS, 129, 399

van Langevelde, H.J., van Dishoeck, E.F., van der Werf, P.P., & Blake, G.A. 1994, A&A, 287, L25

Walter, F.M. & Liu, Y. 1997, in " The Scientific Impact of the Goddard High Resolution Spectrograph", eds. J.C. Brandt, C.C. Petersen, & T.B. Ake, ASP Conference Series # 143 (San Francisco: ASP), p. 360

White, R.J. & Ghez, A.M. 2001, ApJ, 556, 265

Wilkinson, E., Harper, G.H., Brown, A., & Herczeg, G.J. 2002, AJ, 124, 1077

Wolfire, M.G. & Konigl, A. 1991, ApJ, 383, 205

Wood, B.E., Karovska, M., & Raymond, J.C. 2002, ApJ, 575, 1057

Fig. 1.— The two-dimensional long-slit spectrum of T Tau, obtained on 2000 December 1, at a position angle of 345°. The spatial (Y) axis is in arcseconds along the slit, with positive Y corresponding to larger pixel numbers on the chip. The spatial axis corresponds approximately to the distance north of T Tau N. The intensity of the emission within $0.25''$ of T Tau N has been reduced by a factor of 100 to show details near the star. The intensity scaling is linear. The dark vertical stripe at λ1216 Å is geocoronal Ly α emission; the notch $12''$ above T Tau is an occulting bar in the STIS. The weaker geocoronal O I λ1304 Å emission is also evident. Emission in the strongest lines can be traced $9''$ to the south. Note the spatial structure of the intensity.

Fig. 2.— The two-dimensional long-slit spectrum of T Tau, obtained on 2000 November 26, at a position angle of 100° (West on the sky is a positive offset along the spatial axis.) Details are as in Fig. 1. Emission in the strongest lines can be seen up to $7''$ west of the star.

Fig. 3.— The on-source spectrum from 2001 December 1. This is extracted from three spatial pixels centered on T Tau N. The strongest line is a blend of C IV and H_2. Line identifications are given in Table 2.

Fig. 4.— The region of H I Ly α in the stellar spectra. The spectra are 7 spatial pixels wide centered on T Tau N. The thick solid lines, the dotted line, and the dashed lines are the spectra observed on December 1, November 26, and January 5, respectively. The dash-dot trace is the mean geocoronal Ly α spectrum, which has been subtracted. The emission lines at 1206 and 1238 Å are, respectively, Si III and N V. The emission lines and the continuum are uniformly 30% brighter on December 1. The stellar Ly α flux is not detected on January 5.

Fig. 5.— Upper panel: the ratio of the stellar flux (within $0.085''$ of the star) in the December 1 observation to that on November 26. The continuous line is a fit to the smoothed data. The continuum is uniformly brighter by about 30% shortward of 1600 Å, while the strong transition region lines are enhanced about a factor of 2, on December 1. This could be a consequence of increased accretion at that time. Lower panel: the ratio of the stellar flux on 1 December to that on January 5. The continuous line is a fit to the smoothed data. The continuum is enhanced, as in the upper plot, but there are more complex flux variations in the lines. Relative to the January 5 spectrum, on December 1 H I Ly α is much more strongly enhanced relative to the transition region lines, while the cool wind lines (λ1300 Å O I and the λ1350 Å complex) are reduced.

Fig. 6.— The on-source spectrum of T Tau (bottom solid line) and the spectrum of the Southern Knot of T Tau (top solid line, offset by 5 and increased in brightness by a factor of 5), from the December 1 observation. The synthetic H_2 spectrum (dotted lines) demonstrates

that all of the emission lines in the Southern Knot and many of the lines in the on-source spectrum result from H_2 fluorescence. The brightest H_2 lines in the on-source spectrum are not detected in the Southern Knot.

Fig. 7.— Comparison of the observed spatial profiles of the H_2 lines in the R(3)/P(5) and R(6)/P(8) progressions (thick line), the stellar lines (thin line) and the reference point source profile (AR UMa; dotted line). These data are for the 345° position angle; the profiles at the 10° position angle are similar. To the north (positive displacement) the H_2 emission is clearly extended, while the stellar lines appear to be enhanced relative to the reference profile. To the south the Southern Knot at -1.3″ is prominent in both sets of lines. There is no evidence for significant extended emission between the Southern Knot and the star (the apparent excess in the H_2 emission above the reference profile between -0.5 and -0.7″ can be accounted for by scattering from the Southern Knot), as would be expected if that region is shadowed by a foreground obscuration.

Fig. 8.— The spatial profiles on an expanded scale to show the behavior close to the star. The H_2 profile is the thick solid line; the stellar line profile is the thin solid line. The two reference profiles are plotted as dotted lines. The lower reference profile is a point source without any background; the upper reference profile is the same point source but superposed upon a flat background fit to the H_2 profile at -1.4 and +0.4″. The latter reference profile should be compared with the H_2 profile. The H_2 and stellar line profiles are broader than the reference profiles.

Fig. 9.— As Figure 7, but for the 100° orientation observation. East is to the left (negative displacement).

Fig. 10.— A simple model (smooth curve between -2 and $+3$ arcsec) for the spatial distribution of the extended H_2 emission in the north-south direction. The extended emission is modeled as a linear brightness disribution. The dip at -0.62″, near the position of T Tau S, has a half width of 0.32″, sharp edges, and is black at the center prior to convolution with the instrumental resolution. This model is invalid outside the plotted range.

Fig. 11.— Comparison of the spatial profiles at position angles of 345° (thick line) and 10° (thin line). Fluxes are normalized to the peak flux in the December 1 (345°) observation. The dip near -0.7″ is displaced to greater negative positions, and is somewhat broader, in the 10° cut.

Fig. 12.— The logarithmically-scaled total observed intensity in the spatially resolved far UV spectra, overlaid on the optical reflected light contours (Stapelfeldt et al. 1998). To the north and the east the far UV flux does not extend beyond the edges of the reflected light, while

the Southern Knot coincides with the HH 255 outflow. H_2 emission seems to fill the open cavity to the west. The plus marks the position of T Tau S.

Table 1. Observing Log

Root	Date	Aperture	Grating	Exposure (s)	PA °
o5e301	2000 Dec 01	52x0.2	G140L	6800	345
o5e302	2000 Nov 26	52x0.2	G140L	6800	100
o5e303	2001 Jan 05	52x0.2	G140L	7200	10
o5e304	2000 Sep 08	0.2x0.06	E140M	12080	–

Table 2. Strong Lines in the on-Source Spectrum

Wavelength	ID	Flux[a] (10^{-15} erg cm^{-2} s^{-1})	
1175.4	C III	8.7	
1206.3	Si III	8.2	
1220	H I		b
1238.5	N V, H_2 2-2 R(11)	18.6	
1265.6	C I, H_2 4-1 P(19)	5.6	
1270.5	S I, H_2 2-2 P(13), 2-2 R(14)	3.0	
1274.4	H_2 0-3 R(0), 0-3 R(1)	7.5	
1282.8	H_2 0-3 P(3)	4.2	
1295.7	S I	26.4	
1302.9	O I	41.8	
1305.9	S I, O I	36.6	
1309.3	Si II	18.5	
1324.8	H_2 2-3 R(14)	3.0	
1335.5	C II, H_2 0-4 R(0), 0-4 R(1), 0-4 P(2)	35.1	c
1341.8	H_2 0-4 P(3)	11.1	
1351.5	Cl I	3.1	
1355.3	O I,C I	5.4	
1359.4	C I	9.9	
1365.9	H_2 4-3 P(19)	4.0	
1371.1	H_2 2-5 P(16)	2.8	
1393.7	Si IV, H_2 0-5 R(0), 0-5 R(1)	34.9	
1399	H_2 0-5 P(2)		d
1401.8	Si IV, H_2 0-5 P(3)	47.6	
1434.8	H_2 2-5 P(13)	14.1	
1444.9	H_2 1-6 P(5)	5.0	
1455.1	H_2 0-6 R(1), 0-6 R(2), 2-6 R(11)	20.9	
1463.9	H_2 0-6 P(2), 0-6 P(3)	21.1	
1472.3	S I	19.2	
1482.5	S I, H_2 0-6 R(14)	5.1	
1485.6	S I, H_2 0-5 P(13)	2.8	

Table 2—Continued

Wavelength	ID	Flux[a] (10^{-15} erg cm^{-2} s^{-1})
1488.7	H_2 1-7 R(3)	7.5
1504.9	H_2 1-7 P(5)	7.7
1516.4	H_2 0-7 R(0), 0-7 R(1)	7.3
1525.3	H_2 0-7 P(3), Si II	11.6
1534.5	Si II	6.0
1547.8	C IV	111.
1550.6	C IV	44.9
1555.5	H_2 2-8 R(11)	3.2
1562.2	H_2 1-8 P(5)	4.5
1588.7	H_2 2-8 P(13)	6.5
1602.1	H_2 2-9 R(11)	15.7
1632.1	H_2 2-9 P(13)	5.5
1640.4	He II	52.3
1649.0	Fe II	1.5
1660.0	O III]	6.4
1665.6	O III]	14.1

[a]Fluxes observed on 1 December 2000. Fluxes of blended lines were measured by fitting multiple Gaussians.

[b]Combination of geocoronal and stellar Ly α. See §3.2.1.

[c]Unresolved doublet.

[d]The line is noticeable on wing of Si IV line, but flux cannot be measured accurately at this dispersion.

Table 3. H_2 Progressions in the on-Source Spectra

Wavelength (Å)	ID	Blend[a]
Pumped by 2-1 P(13) at 1217.904		
1271	2-2 P(13)	H_2
1325	2-3 P(13)	H_2
1434	2-5 P(13)	
1556	2-8 R(11)	
1589	2-8 P(13)	
1602	2-9 R(11)	
1632	2-9 P(13)	
Pumped by 0-2 R(1) at 1217.643		
1275	0-3 R(1)	H_2
1283	0-3 P(3)	
1334	0-4 R(1)	C II, H_2
1342	0-4 P(3)	
1394	0-5 R(1)	Si IV, H_2
1403	0-5 P(3)	Si IV
1455	0-6 R(1)	H_2
1464	0-6 P(3)	
1516	0-7 R(1)	H_2
1525	0-7 P(3)	
1576	0-8 R(1)	
Pumped by 1-2 P(5) at 1216.070		
1431	1-6 R(3)	
1446	1-6 P(5)	
1490	1-7 R(3)	

Table 3—Continued

Wavelength (Å)	ID	Blend[a]
1505	1-7 P(5)	
1562	1-8 P(5)	
Pumped by 0-2 R(0) at 1217.205		
1274	0-3 R(0)	H_2
1279	0-3 P(2)	H_2
1333	0-4 R(0)	C II, H_2
1338	0-4 P(2)	C II, H_2
1394	0-5 R(0)	Si IV, H_2
1399	0-5 P(2)	Si IV
1455	0-6 R(0)	H_2
1460	0-6 P(2)	
1516	0-7 R(0)	H_2
1521	0-7 P(2)	
Pumped by 2-1 R(14) 1218.536		
1257	2-1 P(16)	
1271	2-2 R(14)	H_2
1324	2-3 R(14)	H_2
1481	2-6 R(14)	S I
Pumped by 4-0 P(19) 1217.410		
1267	4-1 P(19)	
1274	4-2 R(17)	H_2
1372	4-4 R(17)	
Pumped by 0-3 R(2) 1219.089		

Table 3—Continued

Wavelength (Å)	ID	Blend[a]
1407	0-5 P(4)	
Pumped by 2-2 R(9) 1219.089		
1573	2-8 R(9)	
1592	2-9 R(9)	
Pumped by 2-2 P(8) 1219.154		
1579	2-9 R(6)	

[a]Other species in line blend

Table 4. Strong Features in the Southern Knot

Wavelength (Å)	ID
1238.0	P(8) 1-2
1258.0	R(3) 1-3
1272.5	P(5) 1-3 + R(6) 1-3
1293.7	P(8) 1-3
1315.2	R(3) 1-4
1373.0	R(3) 1-5
1387.6	P(5) 1-5
1432.0	R(3) 1-6
1443.0	R(6) 1-6 + P(5) 1-6
1446.5	P(5) 1-6 + R(6) 1-6
1467.5	P(8) 1-6
1489.9	R(3) 1-7
1500.5	R(6) 1-7
1504.5	P(5) 1-7
1524.9	P(8) 1-7
1547.3	R(3) 1-8
1557.0	R(6) 1-8
1562.9	P(5) 1-8
1579.5	P(8) 1-8
1603.1	R(3) 1-9
1618.3	P(5) 1-9

Table 5. Features Used for Spatial Profile Analysis

Wavelength (Å)	ID
Wavelengths of stellar lines	
1176.3	C III
1206.5	Si III
1239.2	N V + H_2
1336.2	C II + H_2
1357.7	C I + O I
1394.2	Si IV + H_2
1401.6	Si IV + H_2
1455.4	H_2 R(0) 0-6
1472.3	S I
1547.3	C IV + H_2
1590.4	H_2
1641.9	He II
1666.3	C I + Fe II + O III]
Continuum regions	
1682.2 ± 10.2	
1707.5 ± 2.8	

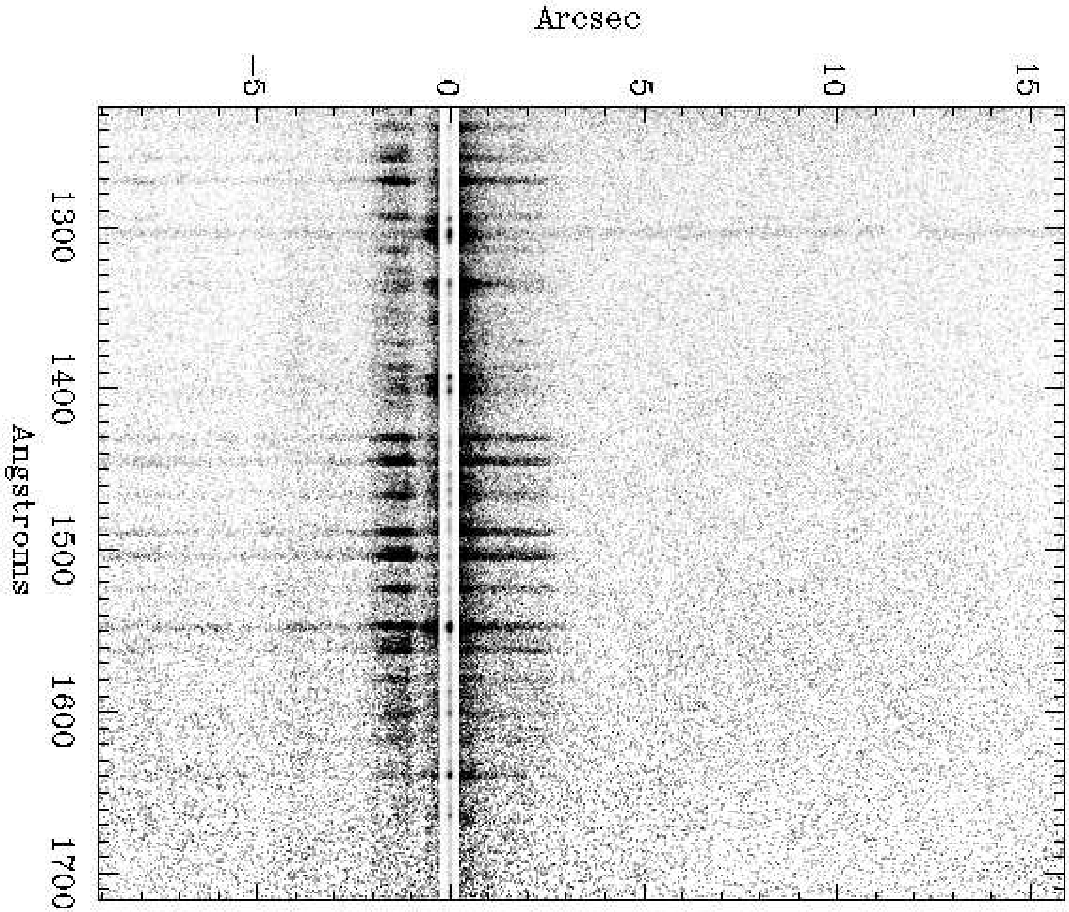
Arcsec
−5
0
5
10
15
1300
1400
1500
1600
1700
Angstroms

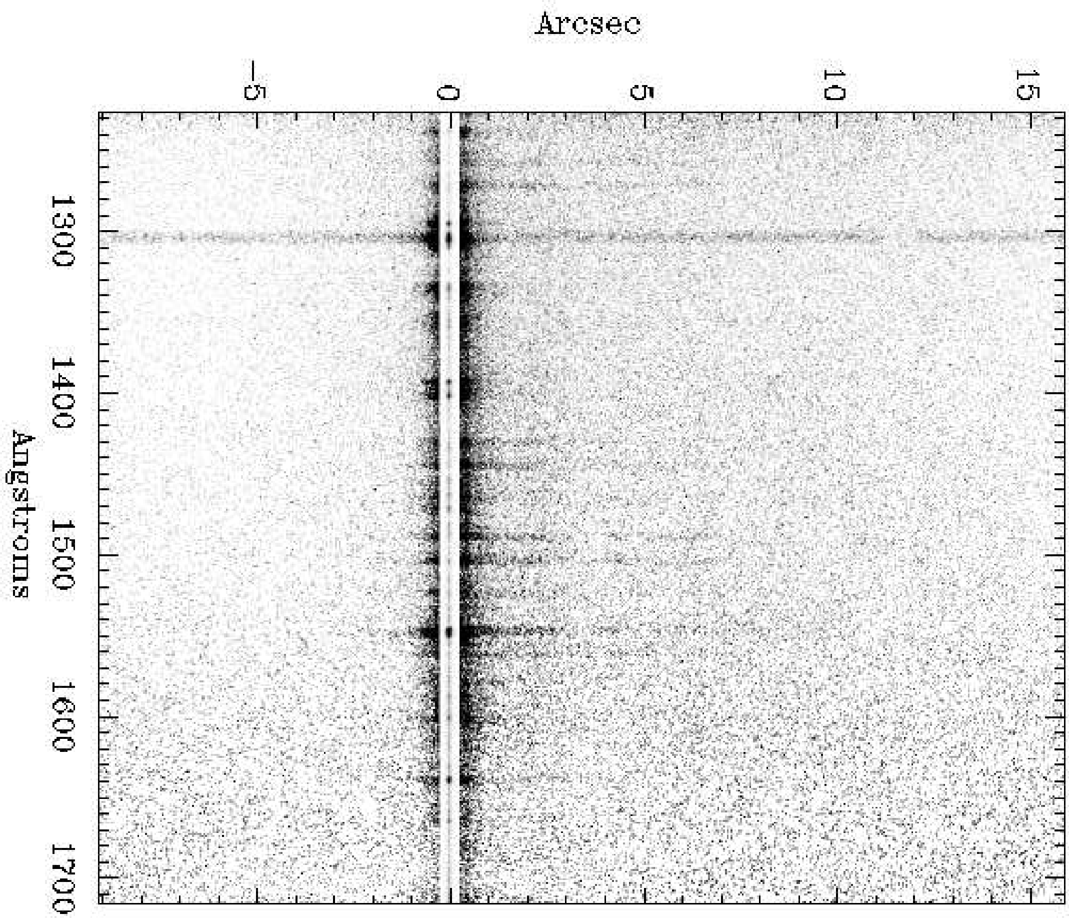

Arcsec
−5
0
5
10
15
1300
1400
1500
1600
1700
Angstroms

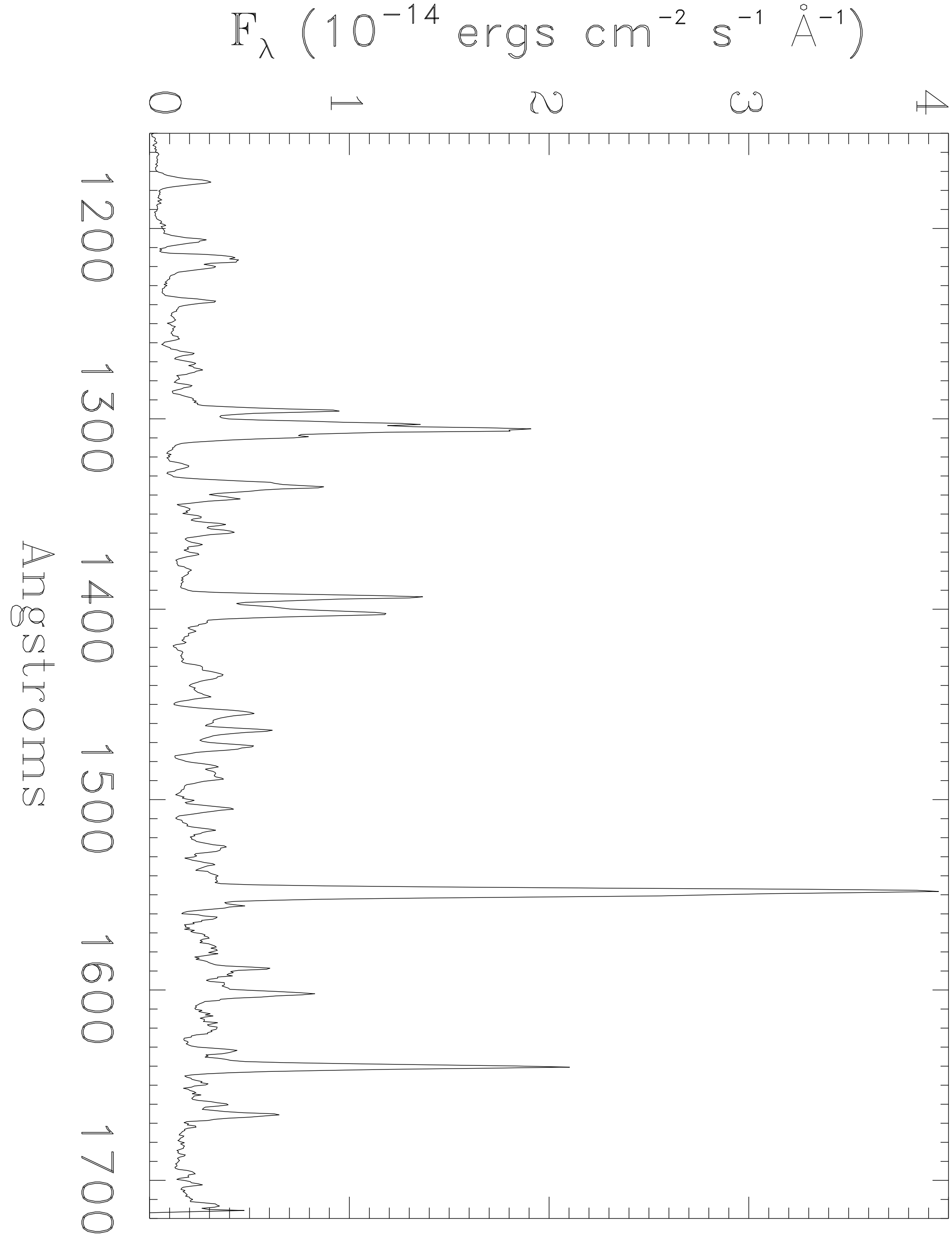

F_λ (10^{-14} ergs cm^{-2} s^{-1} Å^{-1})
0
1
2
3
4
1200
1300
1400
1500
1600
1700
Angstroms

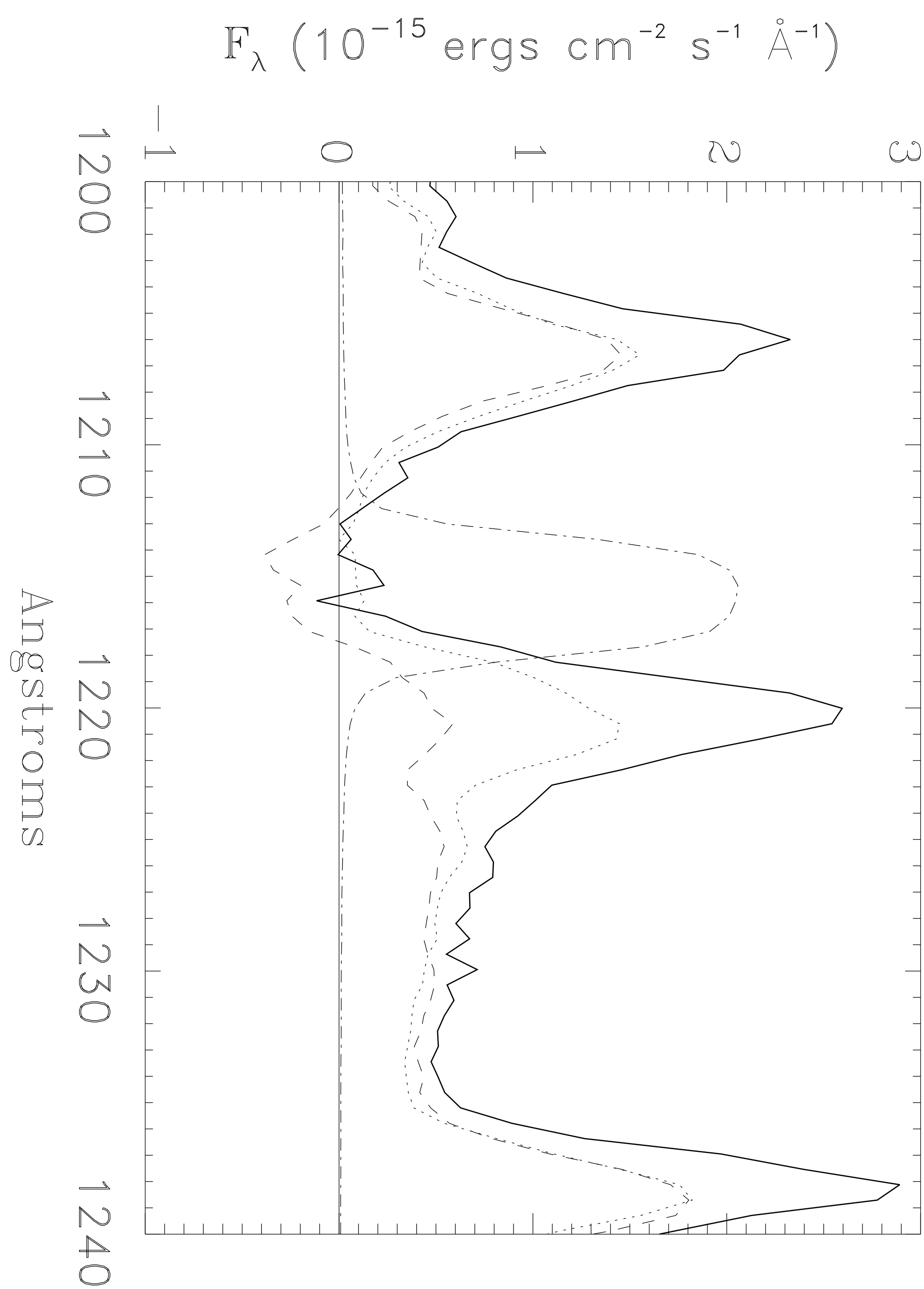

F$_\lambda$ (10^{-15} ergs cm^{-2} s^{-1} Å^{-1})
−1
0
1
2
3
1200
1210
1220
1230
1240
Angstroms

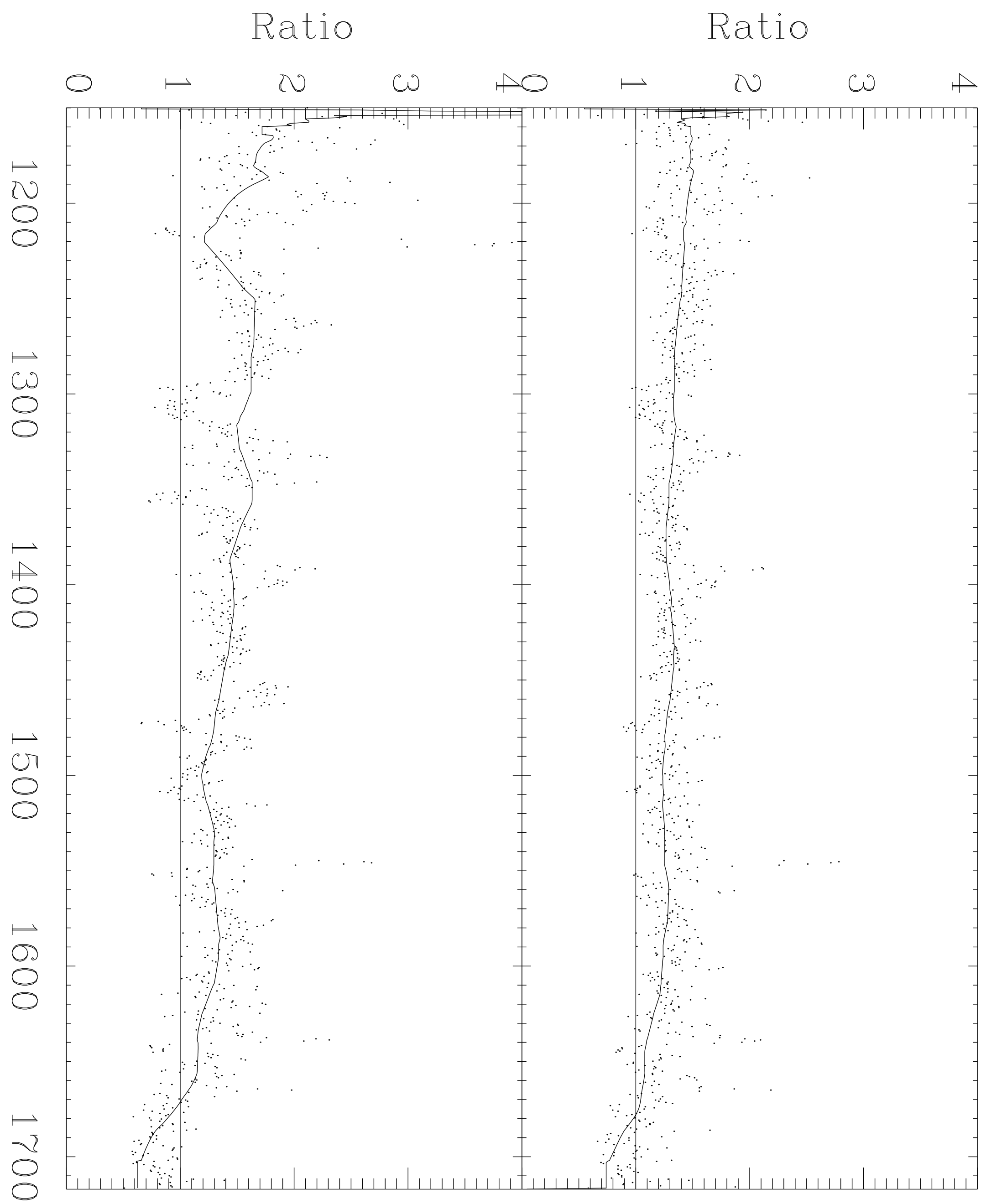
Ratio
Ratio
0
1
2
3
4
1200
1300
1400
1500
1600
1700

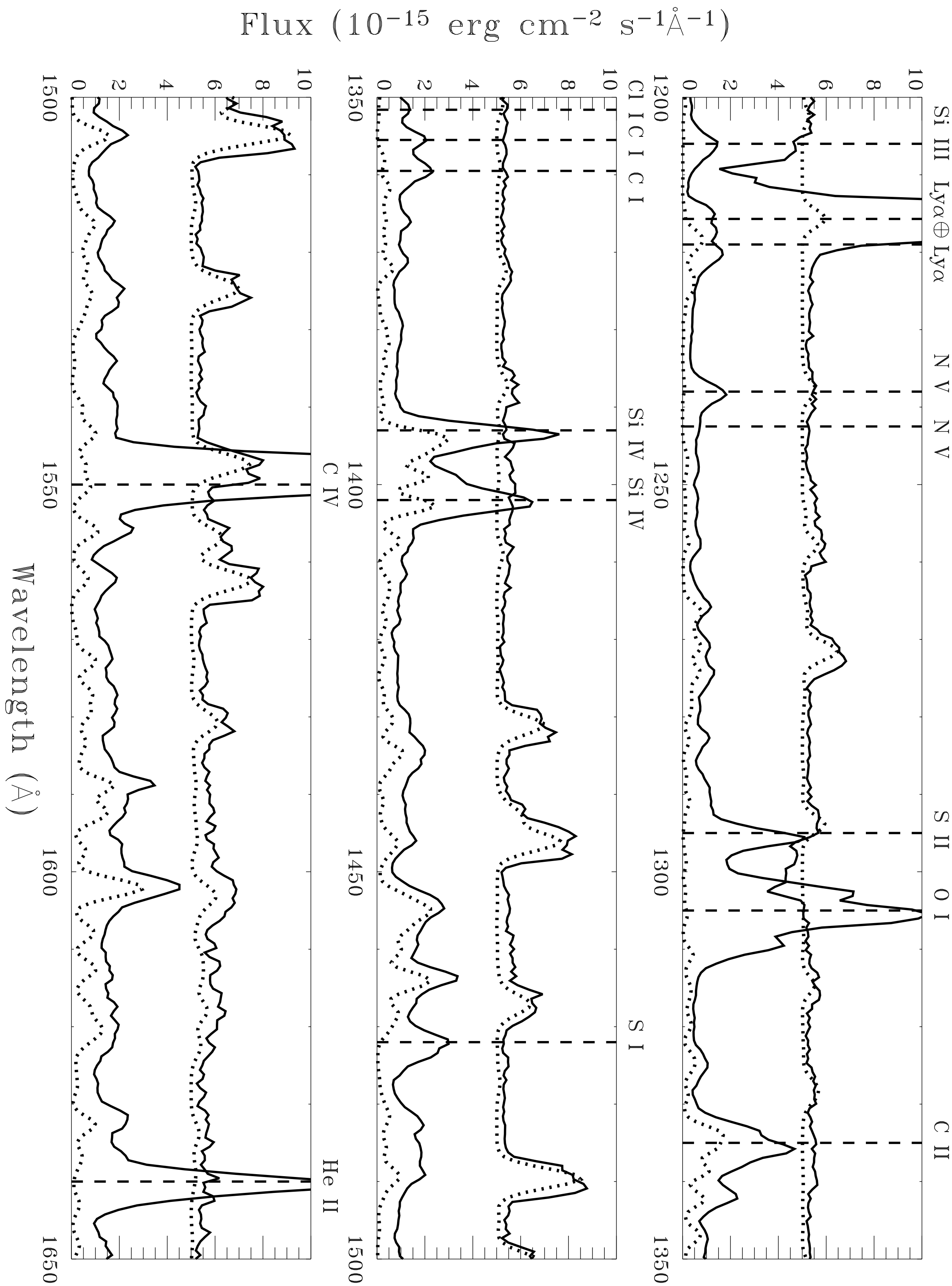

Flux (10^{-15} erg cm^{-2} s^{-1}Å^{-1})
Wavelength (Å)
Si III
Ly$\alpha\oplus$Lyα
N V
N V
S II
O I
C II
C I
C I
C I
Si IV
Si IV
S I
C IV
He II
1200
1250
1300
1350
1400
1450
1500
1550
1600
1650
0
2
4
6
8
10

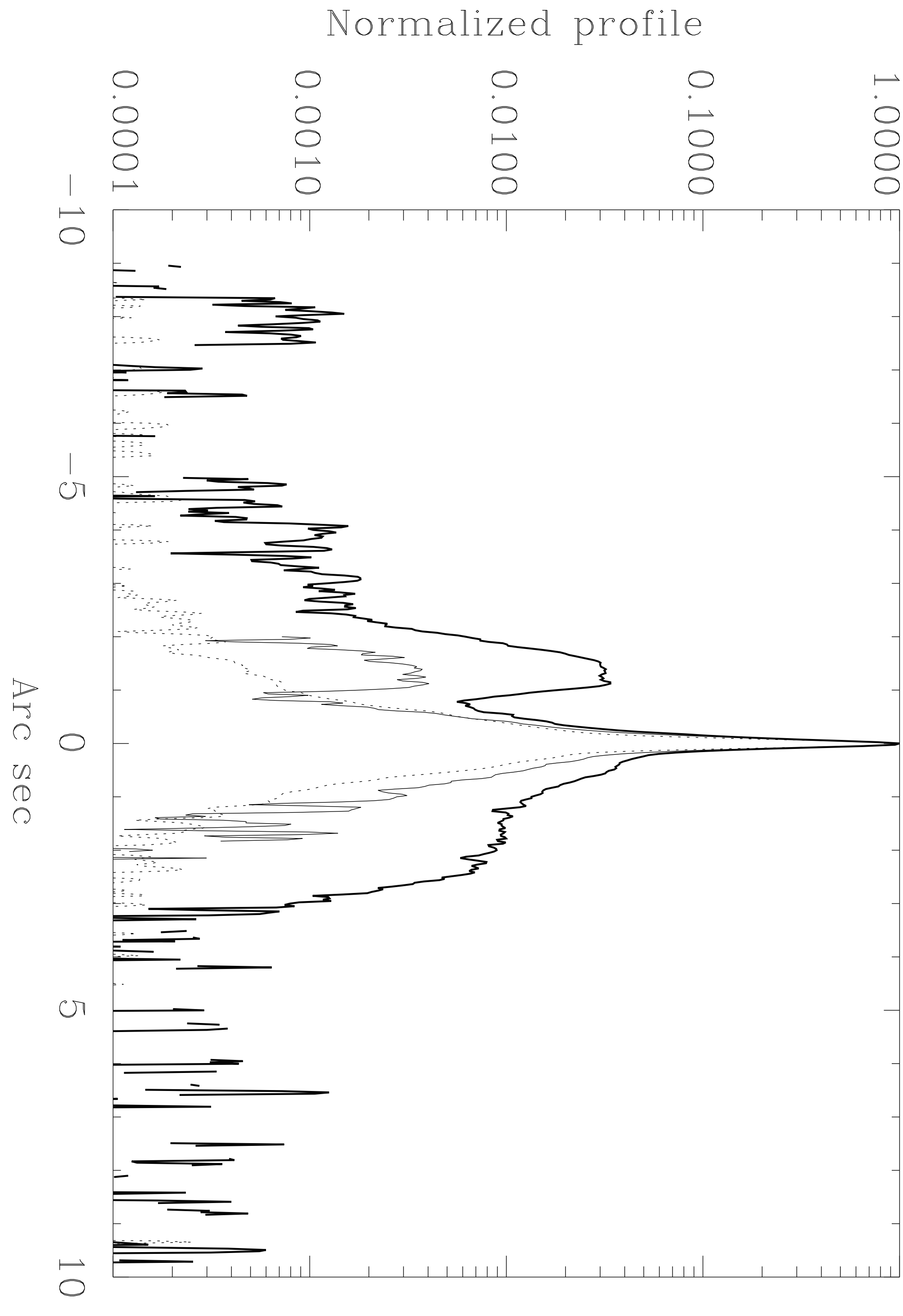
Normalized profile
1.0000
0.1000
0.0100
0.0010
0.0001
−10
−5
0
5
10
Arc sec

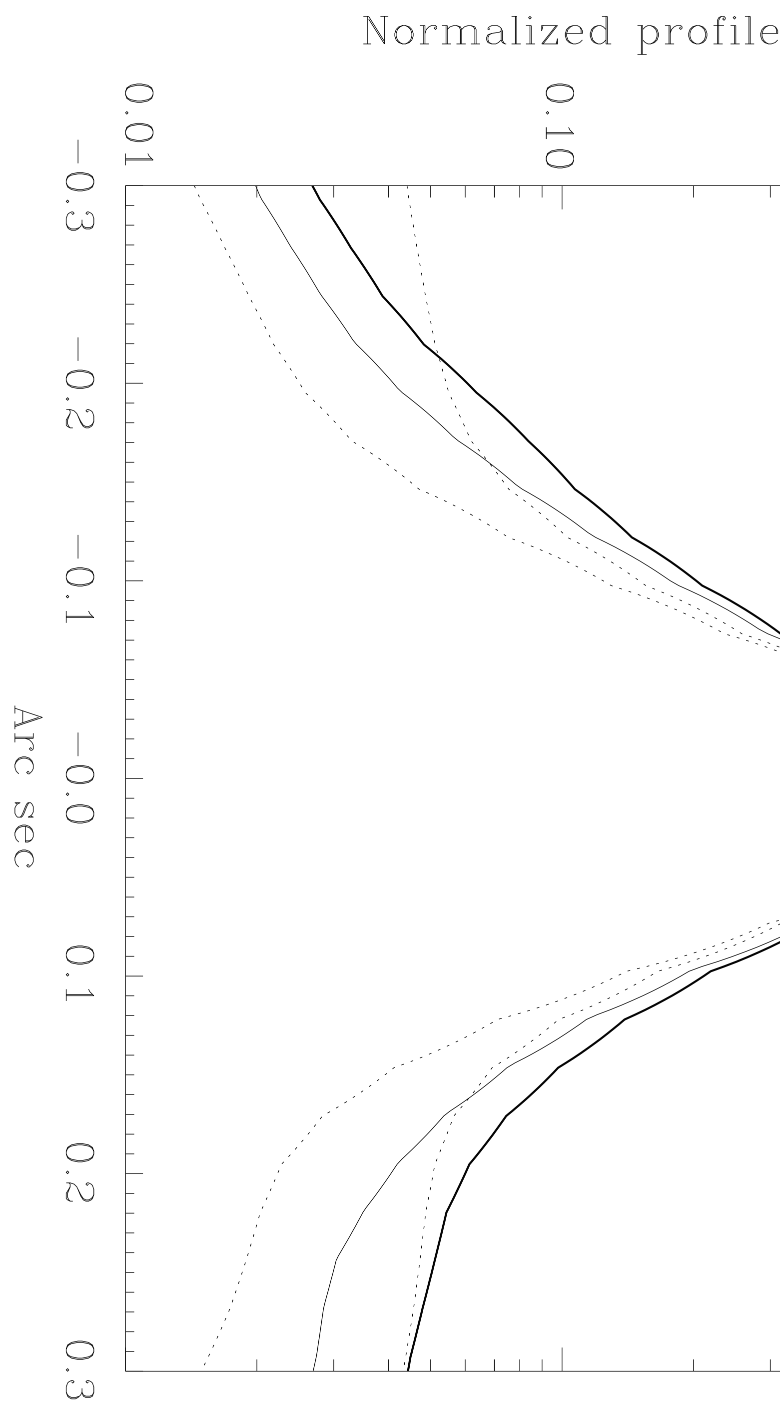

Normalized profile
0.01
0.10
1.00
−0.3
−0.2
−0.1
−0.0
0.1
0.2
0.3
Arc sec

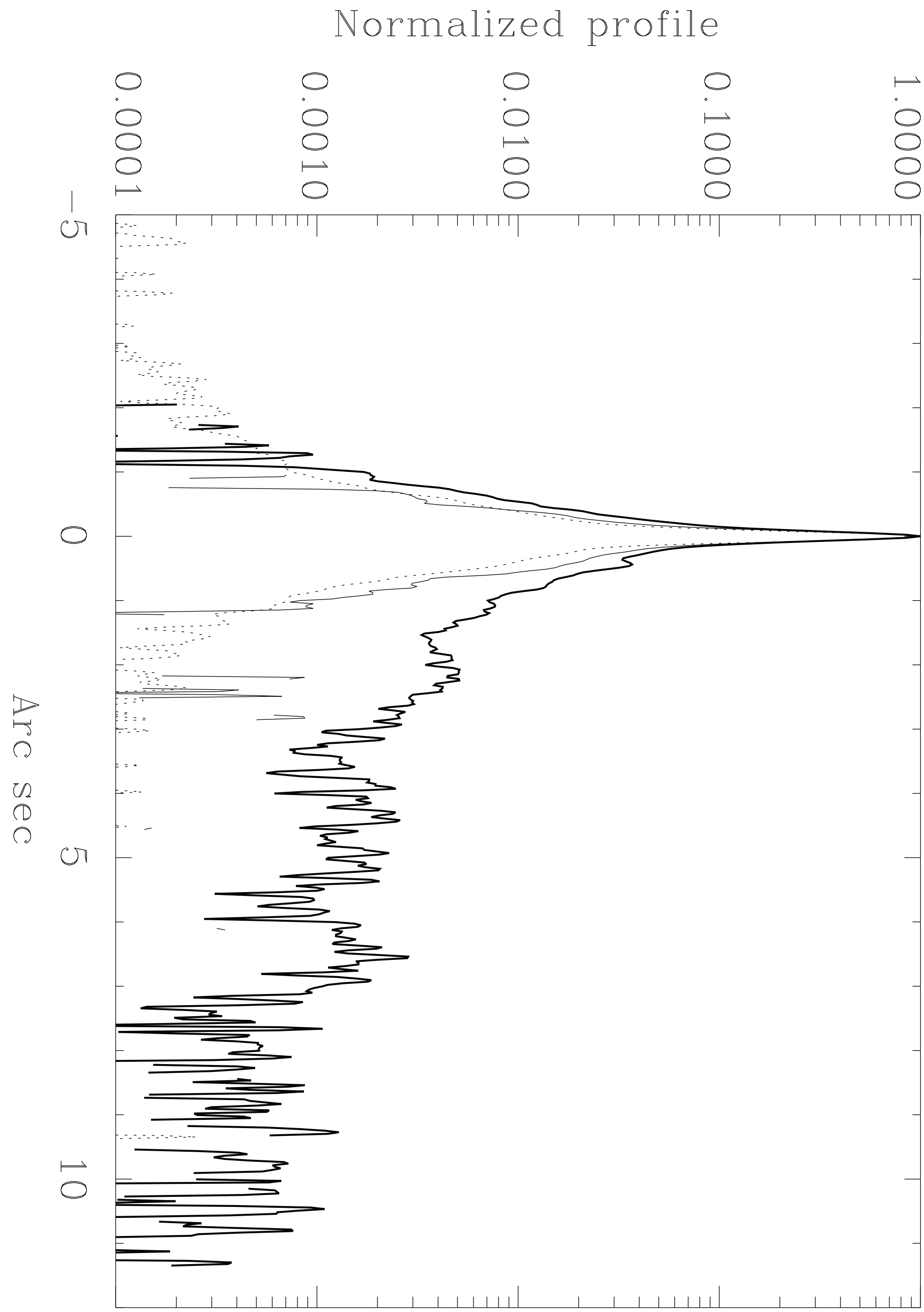
Normalized profile
1.0000
0.1000
0.0100
0.0010
0.0001
−5
0
5
10
Arc sec

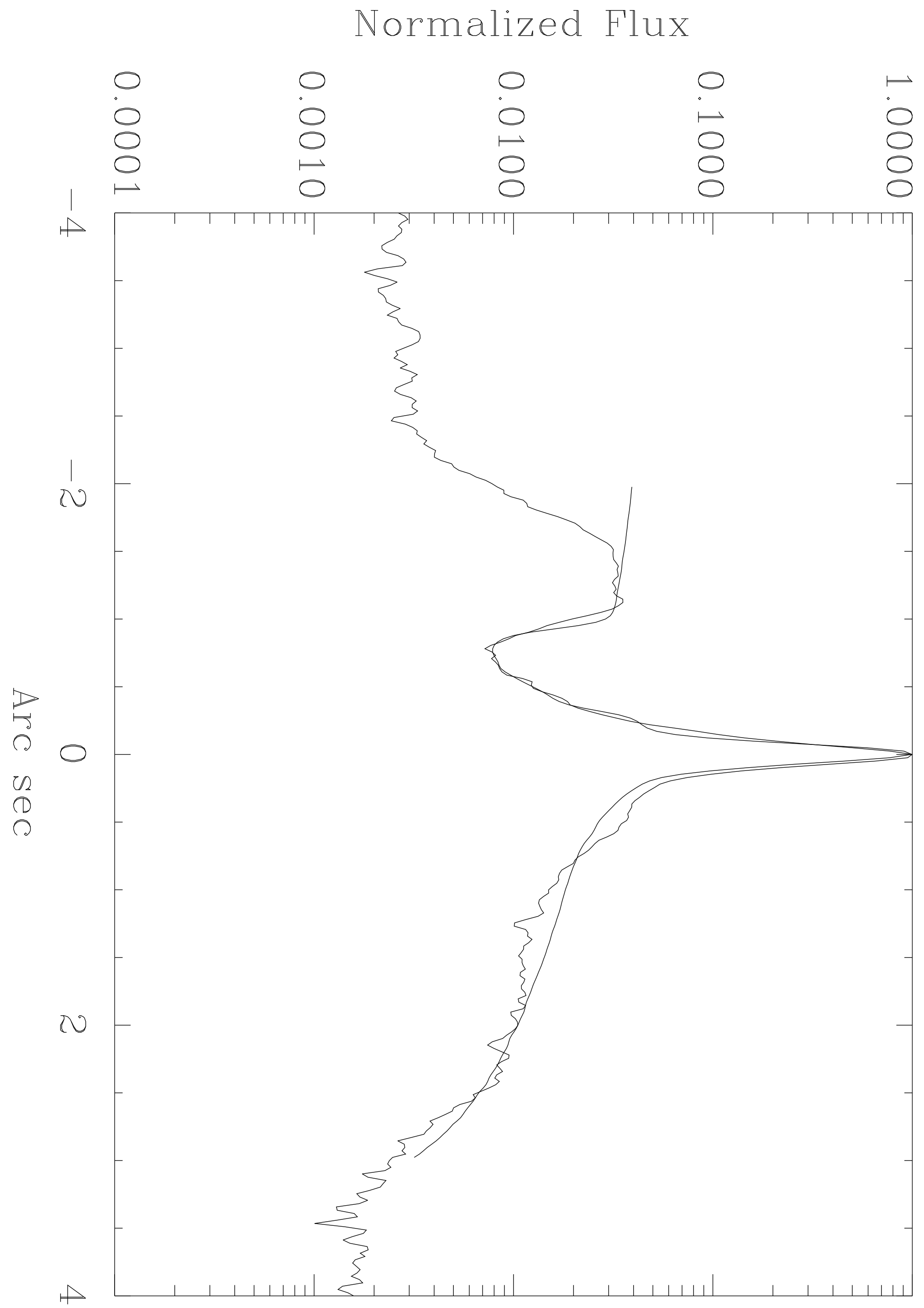
Normalized Flux
0.0001
0.0010
0.0100
0.1000
1.0000
Arc sec
−4
−2
0
2
4

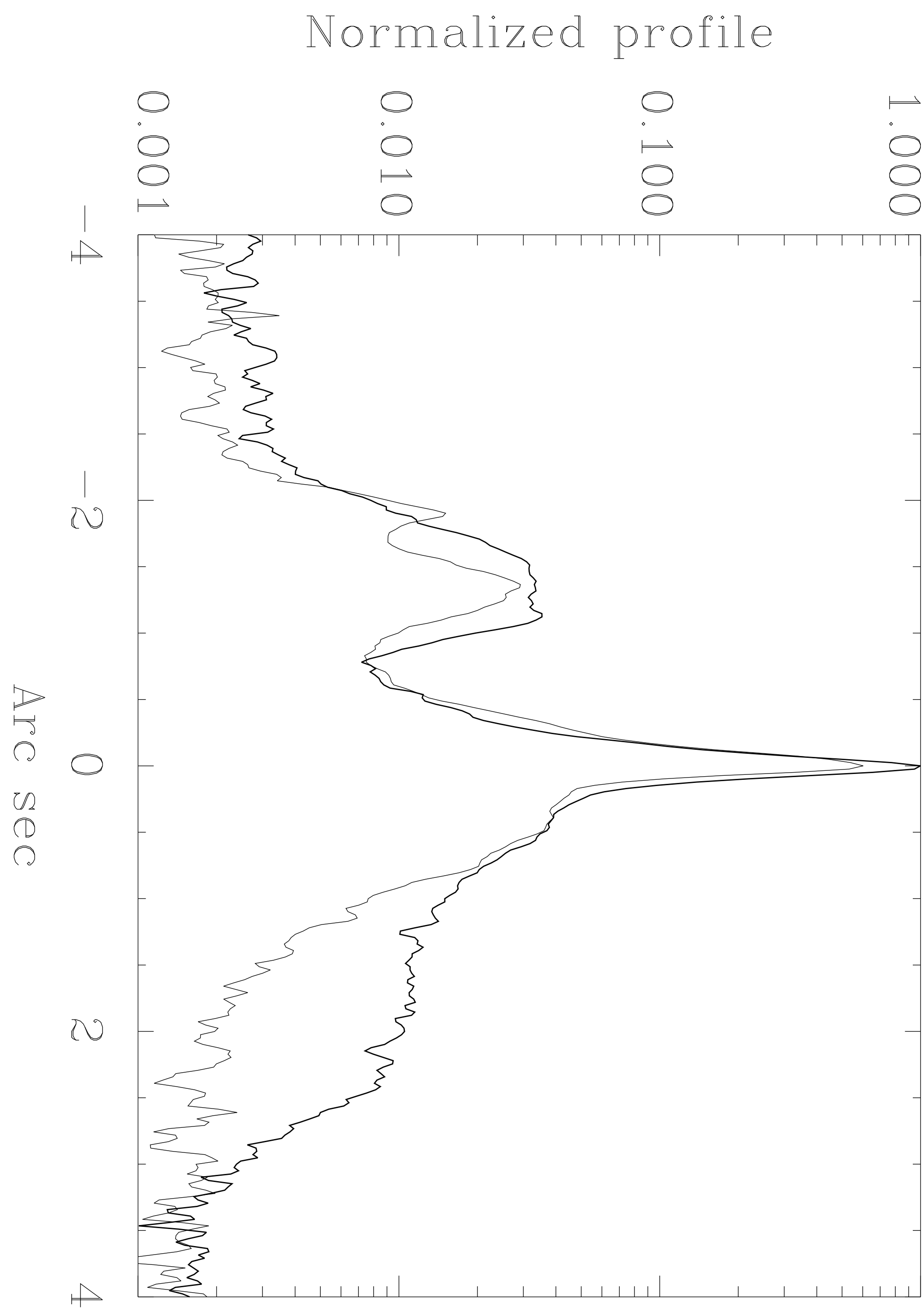
Normalized profile
0.001
0.010
0.100
1.000
−4
−2
0
2
4
Arc sec

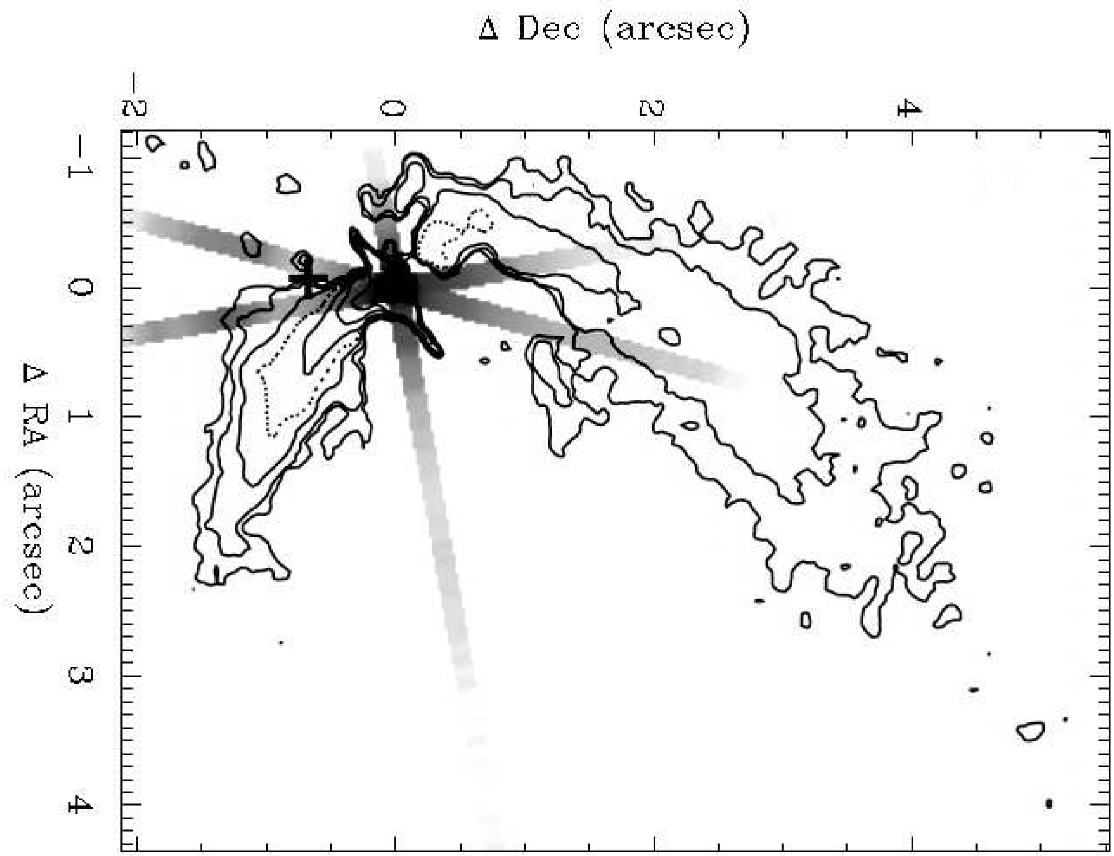
Δ Dec (arcsec)
−2
0
2
4
Δ RA (arcsec)
−1
0
1
2
3
4